AIMS Mathematics, 11(5): 13710–13743.
DOI: 10.3934/math.2026565
Received: 12 March 2026
Revised: 18 April 2026
Accepted: 24 April 2026
Published: 15 May 2026

http://www.aimspress.com/journal/Math

Research article

An enhanced ultraspherical collocation framework with Chebyshev nodes for the time-fractional FitzHugh–Nagumo equation

Youssri Hassan Youssri[1], Muhammad Mujtaba Shaikh[2], Iqbal M. Batiha[3,4,*], Nidal Anakira[5], Irianto Irianto[6] and Tala Sasa[7]

[1] Department of Mathematics, Faculty of Science, Cairo University, Giza 12613, Egypt

[2] Department of Basic Sciences and Related Studies, Mehran University of Engineering and Technology, Jamshoro 76062, Pakistan

[3] Department of Mathematics, Al Zaytoonah University of Jordan, Amman 11733, Jordan

[4] Nonlinear Dynamics Research Center (NDRC), Ajman University, Ajman 346, UAE

[5] Mathematics Education Program, Faculty of Education and Arts, Sohar University, Sohar 311, Oman

[6] Department of General Education, Faculty of Resilience, Rabdan Academy, Abu Dhabi, United Arab Emirates

[7] Department of Mathematics, Faculty of Science, Private Applied Science University, Amman, Jordan

* **Correspondence:** Email: i.batiha@zuj.edu.jo.

Abstract: This work introduces a novel spectral collocation scheme based on ultraspherical (Gegenbauer) polynomials evaluated at Chebyshev–Gauss–Lobatto nodes for the numerical treatment of the nonlinear inhomogeneous time-fractional FitzHugh–Nagumo differential problem. The proposed methodology exploits the flexibility of the ultraspherical parameter $\lambda > -\frac{1}{2}$ to achieve enhanced accuracy and stability. We derived new operational matrices for both integer-order and Caputo fractional derivatives of the shifted ultraspherical basis, accompanied by rigorous proofs. A comprehensive convergence analysis in the L^2 norm was established, demonstrating spectral accuracy. Extensive numerical experiments confirmed that the proposed method outperforms the classical Legendre-based approach for optimal choices of λ, with errors reduced by several orders of magnitude. The superiority of optimized λ over the Legendre case ($\lambda = \frac{1}{2}$) was demonstrated through both numerical benchmarks and theoretical error bounds that explicitly depend on λ, showing that the Legendre choice is not universally optimal for problems with boundary layers or specific regularity properties. An efficient algorithmic implementation was provided, and comparative tables illustrate the superiority of the ultraspherical framework across various fractional orders and parameter settings.

Keywords: ultraspherical polynomials; Chebyshev nodes; time-fractional FitzHugh–Nagumo equation; spectral collocation; operational matrices; L^2-convergence; error analysis
Mathematics Subject Classification: 33C45, 65N35, 65L60, 35R11

1. Introduction

Spectral methods constitute a powerful class of numerical techniques for approximating solutions to differential equations of diverse types [1, 2]. The fundamental principle underlying these methods is the representation of the unknown solution as a truncated series of globally smooth basis functions, typically orthogonal polynomials. Compared to local discretization schemes, spectral approaches offer exponential convergence for smooth problems and superior resolution per degree of freedom [3, 4].

Among the various spectral formulations, collocation methods are particularly attractive due to their simplicity of implementation and flexibility in handling nonlinear terms and complex boundary conditions [5]. The choice of basis functions and collocation points critically influences the accuracy, stability, and efficiency of the resulting scheme. While Legendre and Chebyshev polynomials have been extensively employed, the broader family of ultraspherical (Gegenbauer) polynomials $C_n^{(\lambda)}(x)$, parameterized by $\lambda > -\frac{1}{2}$, provides a valuable continuum of bases that can be tuned to the problem at hand [6, 7].

Recent advances in spectral methods for fractional partial differential equations have been comprehensively surveyed in [8, 9]. These works highlight the growing interest in adaptive basis selection and parameter optimization for fractional operators, motivating our focus on the ultraspherical parameter λ as a tunable degree of freedom.

The two- and higher-point differential equations subjected to initial and/or boundary conditions model system dynamics and oscillations in a better way [10]. Often, such problems appear as a constraint in more advanced optimal control problems [11]. The Van der Pol and Duffing oscillators exhibit nonlinear characteristics, which cannot be understood fully using an analytic method [12, 13]. The nonlinearities and complexities of the models often demand efficient numerical treatment to acquire stable and accurate solutions [14, 15]. An exhaustive understanding of the dynamics is offered by studying the local, non-local, and memory-based fractional extensions of these models [16, 17]. When these models are generalized further, we often get more sophisticated models like the fractional FitzHugh–Nagumo equation, which is a generalization of the Van der Pol oscillator in a fractional sense [18, 19].

The time-fractional FitzHugh–Nagumo equation models excitable media and nerve impulse propagation, incorporating memory effects through fractional temporal derivatives [20–22]. Its numerical solution poses challenges due to the nonlocal nature of fractional operators coupled with strong nonlinearity. Recent contributions have addressed this problem using various polynomial bases [23, 24]. In [25], a collocation method was used along the Chebyshev basis, while in some studies [26, 27], authors used the shifted Legendre polynomial basis to numerically solve the fractional FitzHugh–Nagumo model utilizing the usual collocation procedure. Despite repeated and similar applications of the method, the potential of ultraspherical polynomials with optimized λ remains largely unexplored. Ultraspherical polynomials provide a generalized basis and assist in a flexible

solution of such problems based on the optimal parameter λ.

The principal novelty of this work lies in: (i) the systematic derivation of operational matrices for ultraspherical polynomials with arbitrary λ, extending beyond the classical Legendre/Chebyshev cases; (ii) the rigorous L^2-convergence analysis that explicitly quantifies the dependence of error constants on λ; and (iii) the demonstration that adaptive selection of λ can yield order-of-magnitude improvements for problems with boundary layers or specific regularity structures. To position our contribution within the current state-of-the-art research, we note that recent high-performance methods for time-fractional PDEs include the spectral element method of [28], the discontinuous Galerkin approach of [29], and the adaptive wavelet collocation of [30]. While these methods offer complementary advantages, our ultraspherical framework provides a simpler implementation with comparable accuracy for smooth solutions, and superior performance for problems where boundary resolution is critical.

The principal contributions of this manuscript are:

- Development of a shifted ultraspherical basis $C_n^{(\lambda)}(\xi)$ on $[0, 1]$ with explicit power-form and inversion formulas;
- Derivation of novel operational matrices for first/second derivatives and Caputo fractional derivatives of the ultraspherical basis, with complete proofs;
- Formulation of a collocation scheme at Chebyshev–Gauss–Lobatto nodes, ensuring clustering near boundaries for improved resolution of boundary layers;
- Rigorous L^2-convergence analysis establishing spectral accuracy and explicit error bounds dependent on λ;
- Demonstration through numerical benchmarks that the optimal selection of λ yields errors significantly lower than the Legendre case ($\lambda = \frac{1}{2}$);
- Provision of a complete algorithmic description suitable for implementation.

The remainder of this paper is organized as follows. Section 2 reviews essential concepts of fractional calculus and introduces the shifted ultraspherical polynomials with their key properties. Section 3 derives the operational matrices for integer and fractional derivatives. The collocation algorithm for the FitzHugh–Nagumo problem is detailed in Section 4. Section 5 presents the L^2-convergence analysis with proofs. Numerical experiments and comparative results are reported in Section 6. Concluding remarks are given in Section 7.

2. Preliminaries: fractional calculus and ultraspherical polynomials

2.1. Caputo fractional derivative

Definition 2.1. For $\alpha > 0$ with $m - 1 < \alpha \leq m$, $m \in \mathbb{N}$, the Caputo fractional derivative of order α of a sufficiently smooth function $\phi(\tau)$ is defined by [31]

$$ {}^{C}D_{\tau}^{\alpha}\phi(\tau) = \frac{1}{\Gamma(m-\alpha)} \int_0^{\tau} (\tau - s)^{m-\alpha-1} \phi^{(m)}(s)\, ds, \quad \tau > 0. \tag{2.1} $$

In particular, for monomials τ^β with $\beta \in \mathbb{N}_0$,

$$ {}^{C}D_{\tau}^{\alpha}\tau^{\beta} = \begin{cases} 0, & \beta < \lceil \alpha \rceil, \\ \dfrac{\Gamma(\beta+1)}{\Gamma(\beta+1-\alpha)}\,\tau^{\beta-\alpha}, & \beta \geq \lceil \alpha \rceil. \end{cases} \tag{2.2} $$

2.2. *Shifted ultraspherical polynomials*

Throughout this manuscript, we use the terms "ultraspherical polynomials" and "Gegenbauer polynomials" interchangeably, following standard convention in the spectral methods literature [32]. Both refer to the family $C_n^{(\lambda)}(x)$ orthogonal on $[-1, 1]$ with weight $(1 - x^2)^{\lambda-1/2}$.

The ultraspherical (Gegenbauer) polynomials $C_n^{(\lambda)}(x)$, $\lambda > -\frac{1}{2}$, $\lambda \neq 0$, are orthogonal on $[-1, 1]$ with respect to the weight $w^{(\lambda)}(x) = (1 - x^2)^{\lambda-\frac{1}{2}}$:

$$ \int_{-1}^{1} C_m^{(\lambda)}(x) C_n^{(\lambda)}(x)(1 - x^2)^{\lambda-\frac{1}{2}} dx = h_n^{(\lambda)} \delta_{mn}, \tag{2.3} $$

where the normalization constant is

$$ h_n^{(\lambda)} = \frac{\pi\, 2^{1-2\lambda}\Gamma(n + 2\lambda)}{n!(n + \lambda)[\Gamma(\lambda)]^2}. \tag{2.4} $$

For numerical treatment of problems on $[0, 1]$, we introduce the *shifted ultraspherical polynomials*

$$ C_n^{(\lambda)}(\xi) := C_n^{(\lambda)}(2\xi - 1), \quad \xi \in [0, 1]. \tag{2.5} $$

These satisfy the orthogonality relation

$$ \int_0^1 C_m^{(\lambda)}(\xi) C_n^{(\lambda)}(\xi)\, \varpi^{(\lambda)}(\xi)\, d\xi = \frac{h_n^{(\lambda)}}{2^{2\lambda}} \delta_{mn}, \tag{2.6} $$

with the shifted weight $\varpi^{(\lambda)}(\xi) = [\xi(1 - \xi)]^{\lambda-\frac{1}{2}}$.

We emphasize that all symbols and parameters maintain consistent notation throughout: λ denotes the ultraspherical parameter, α the fractional order, N the truncation degree, and $\varpi^{(\lambda)}$ the associated weight function. Any deviation from this convention is explicitly noted.

The power-form expansion of $C_n^{(\lambda)}(\xi)$ is given by [32]

$$ C_n^{(\lambda)}(\xi) = \sum_{k=0}^{n} \mathcal{A}_{n,k}^{(\lambda)} \xi^k, \quad \text{where} \quad \mathcal{A}_{n,k}^{(\lambda)} = \frac{(-1)^{n-k}\Gamma(n + k + 2\lambda)\Gamma(\lambda + \frac{1}{2})}{2^k\, k!\, (n - k)!\, \Gamma(k + 2\lambda)\Gamma(n + \lambda + \frac{1}{2})}. \tag{2.7} $$

Conversely, the inversion formula expressing monomials in the ultraspherical basis reads

$$ \xi^p = \sum_{n=0}^{p} \mathcal{B}_{p,n}^{(\lambda)} C_n^{(\lambda)}(\xi), \quad \mathcal{B}_{p,n}^{(\lambda)} = \frac{(2n + 2\lambda)\Gamma(p + 1)\Gamma(p + 2\lambda)}{2^{2\lambda}\Gamma(n + 2\lambda)\Gamma(p - n + 1)\Gamma(p + n + 2\lambda + 1)} \cdot \frac{\Gamma(\lambda + \frac{1}{2})}{\sqrt{\pi}\,\Gamma(\lambda)}. \tag{2.8} $$

Remark 2.2. The Legendre polynomials correspond to the special case $\lambda = \frac{1}{2}$, for which $C_n^{(1/2)}(\xi) = P_n(2\xi - 1)$. Chebyshev polynomials of the first and second kind are recovered as limiting cases $\lambda \to 0^+$ and $\lambda = 1$, respectively.

2.3. Trial functions satisfying homogeneous boundary conditions

To enforce homogeneous Dirichlet conditions, we define the modified basis functions

$$\Theta_n^{(\lambda)}(\xi) := \xi(1-\xi)\, C_n^{(\lambda)}(2\xi-1), \qquad \chi_n^{(\lambda)}(\tau) := \tau\, C_n^{(\lambda)}(2\tau-1), \quad n = 0, 1, \ldots, \tag{2.9}$$

where $C_n^{(\lambda)}(x)$ denotes the classical Gegenbauer polynomial of degree n and parameter $\lambda > -\frac{1}{2}$, orthogonal on $[-1, 1]$ with respect to the weight $(1-x^2)^{\lambda-\frac{1}{2}}$. The arguments $2\xi - 1$ and $2\tau - 1$ map the unit interval $[0, 1]$ to $[-1, 1]$, yielding the shifted Gegenbauer polynomials $C_n^{(\lambda)}(\xi) := C_n^{(\lambda)}(2\xi - 1)$.

These trial functions satisfy $\Theta_n^{(\lambda)}(0) = \Theta_n^{(\lambda)}(1) = 0$ and $\chi_n^{(\lambda)}(0) = 0$ by construction.

Lemma 2.3. *The trial functions $\{\Theta_n^{(\lambda)}\}$ and $\{\chi_n^{(\lambda)}\}$ are orthogonal with respect to the weighted inner products*

$$\langle \Theta_m^{(\lambda)}, \Theta_n^{(\lambda)} \rangle_{\omega_1} := \int_0^1 \Theta_m^{(\lambda)}(\xi)\Theta_n^{(\lambda)}(\xi)\, \omega_1^{(\lambda)}(\xi)\, d\xi = \gamma_n^{(\lambda)}\delta_{mn}, \tag{2.10}$$

$$\langle \chi_m^{(\lambda)}, \chi_n^{(\lambda)} \rangle_{\omega_2} := \int_0^1 \chi_m^{(\lambda)}(\tau)\chi_n^{(\lambda)}(\tau)\, \omega_2^{(\lambda)}(\tau)\, d\tau = \gamma_n^{(\lambda)}\delta_{mn}, \tag{2.11}$$

where the weight functions are given by

$$\omega_1^{(\lambda)}(\xi) = [\xi(1-\xi)]^{\lambda-\frac{5}{2}}, \qquad \omega_2^{(\lambda)}(\tau) = \tau^{2\lambda-2}(1-\tau)^{\lambda-\frac{1}{2}}, \tag{2.12}$$

and the normalization constants are

$$\gamma_n^{(\lambda)} = \frac{h_n^{(\lambda)}}{2^{2\lambda+2}}, \qquad h_n^{(\lambda)} = \frac{\pi\, 2^{1-2\lambda}\, \Gamma(n+2\lambda)}{n!\,(n+\lambda)\,[\Gamma(\lambda)]^2}. \tag{2.13}$$

Proof. Substituting (2.9) into the left-hand side of (2.10) and using the orthogonality relation for shifted Gegenbauer polynomials,

$$\int_0^1 C_m^{(\lambda)}(2\xi-1) C_n^{(\lambda)}(2\xi-1)\, [\xi(1-\xi)]^{\lambda-\frac{1}{2}}\, d\xi = \frac{h_n^{(\lambda)}}{2^{2\lambda}}\, \delta_{mn}, \tag{2.14}$$

yields the result after straightforward algebraic manipulation. The proof for (2.11) follows analogously, noting that the factor τ in $\chi_n^{(\lambda)}$ modifies the weight to $\omega_2^{(\lambda)}(\tau) = \tau^{2\lambda-2}(1-\tau)^{\lambda-\frac{1}{2}}$. □

3. Operational matrices for derivatives

3.1. Integer-order derivatives

Theorem 3.1. *For $n \geq 1$, the first derivative of the trial function $\Theta_n^{(\lambda)}(\xi)$ admits the expansion*

$$\frac{d}{d\xi}\Theta_n^{(\lambda)}(\xi) = 2 \sum_{\substack{j=0 \\ n+j \text{ odd}}}^{n-1} \mathcal{D}_{n,j}^{(\lambda)}\, \Theta_j^{(\lambda)}(\xi) + \mu_n^{(\lambda)}(\xi), \tag{3.1}$$

where the connection coefficients are

$$\mathcal{D}_{n,j}^{(\lambda)} = \frac{2\lambda + 2j}{2\lambda - 1}\left[2\lambda - 3 + 2\,\frac{j!\,\Gamma(n+2\lambda)}{n!\,\Gamma(j+2\lambda)}\right], \tag{3.2}$$

and the residual term

$$\mu_n^{(\lambda)}(\xi) = C_n^{(\lambda)}(1) \times \begin{cases} 1 - 2\xi, & n \text{ is even}, \\ -1, & n \text{ is odd}, \end{cases} \tag{3.3}$$

with $C_n^{(\lambda)}(1) = \dfrac{\Gamma(n + 2\lambda)}{n!\,\Gamma(2\lambda)}$ *denoting the value of the ultraspherical polynomial at* $x = 1$.

Proof. See [7]. □

Corollary 3.2. *The second derivative satisfies*

$$\frac{d^2}{d\xi^2}\Theta_n^{(\lambda)}(\xi) = 4 \sum_{\substack{k=0 \\ n+k \text{ even}}}^{n-2} \left(\sum_{\substack{j=k+1 \\ j+k \text{ odd}}}^{n-1} \mathcal{D}_{n,j}^{(\lambda)} \mathcal{D}_{j,k}^{(\lambda)} \right) \Theta_k^{(\lambda)}(\xi) + 2 \sum_{\substack{j=0 \\ n+j \text{ odd}}}^{n-1} \mathcal{D}_{n,j}^{(\lambda)} \mu_j^{(\lambda)}(\xi) + \frac{d}{d\xi}\mu_n^{(\lambda)}(\xi), \tag{3.4}$$

which can be written compactly as

$$\frac{d^2}{d\xi^2}\Theta_n^{(\lambda)}(\xi) = \sum_{\substack{k=0 \\ n+k \text{ even}}}^{n-2} \mathcal{E}_{n,k}^{(\lambda)}\, \Theta_k^{(\lambda)}(\xi) + \nu_n^{(\lambda)}(\xi), \tag{3.5}$$

where $\mathcal{E}_{n,k}^{(\lambda)} = 4 \sum_j \mathcal{D}_{n,j}^{(\lambda)} \mathcal{D}_{j,k}^{(\lambda)}$ *and* $\nu_n^{(\lambda)}(\xi) = 2 \sum_j \mathcal{D}_{n,j}^{(\lambda)} \mu_j^{(\lambda)}(\xi) + \frac{d}{d\xi}\mu_n^{(\lambda)}(\xi)$ *is an explicitly computable polynomial of degree at most one.*

Proof. Apply Theorem 3.1 twice. The factor of 2 in (3.1) squares to 4 in the composition, and cross-terms involving $\mu_j^{(\lambda)}$ contribute to the residual $\nu_n^{(\lambda)}$. □

In matrix form, letting $\boldsymbol{\Theta}(\xi) = [\Theta_0^{(\lambda)}(\xi), \ldots, \Theta_N^{(\lambda)}(\xi)]^T$, we have

$$\frac{d}{d\xi}\boldsymbol{\Theta}(\xi) = 2\mathbf{A}^{(\lambda)}\boldsymbol{\Theta}(\xi) + \boldsymbol{\mu}^{(\lambda)}(\xi), \tag{3.6}$$

$$\frac{d^2}{d\xi^2}\boldsymbol{\Theta}(\xi) = 4\left(\mathbf{A}^{(\lambda)}\right)^2 \boldsymbol{\Theta}(\xi) + 2\mathbf{A}^{(\lambda)}\boldsymbol{\mu}^{(\lambda)}(\xi) + \boldsymbol{\nu}^{(\lambda)}(\xi), \tag{3.7}$$

where $\mathbf{A}^{(\lambda)} = (\mathcal{D}_{n,j}^{(\lambda)})$ is a lower-triangular matrix with nonzero entries only when $n > j$ and $n + j$ is odd, and $\boldsymbol{\mu}^{(\lambda)}(\xi)$, $\boldsymbol{\nu}^{(\lambda)}(\xi)$ are vectors of the respective residual terms.

3.2. Caputo fractional derivative operational matrix

We clarify the expansion of fractional powers in the ultraspherical basis. While the inversion formula (2.8) is stated for integer powers, the extension to fractional exponents $\tau^{p+1-\alpha}$ is justified via analytic continuation of the gamma function ratios in $\mathcal{B}_{p,n}^{(\lambda)}$. Specifically, for $\beta = p + 1 - \alpha \notin \mathbb{N}$, we define the expansion coefficients by the same gamma-function expression, which remains well-defined for $\beta > -1$. This approach is consistent with the theory of fractional calculus in weighted Sobolev spaces [8]. The residual term $\Lambda_n^{(\lambda,\alpha)}$ collects contributions from the non-polynomial part of $\tau^{1-\alpha}$ that cannot be represented in the finite basis; only the $p = 0$ term contributes because higher p yield integer shifts that are exactly representable. A detailed justification is provided in Appendix A.2.

Theorem 3.3. *For $0 < \alpha < 1$ and $n \geq 0$, the Caputo derivative of $\chi_n^{(\lambda)}(\tau)$ admits the approximation*

$$ {}^{C}D_{\tau}^{\alpha}\chi_n^{(\lambda)}(\tau) \approx \sum_{\ell=0}^{N} Q_{\ell,n}^{(\lambda,\alpha)}\chi_{\ell}^{(\lambda)}(\tau) + \Lambda_n^{(\lambda,\alpha)}(\tau), \tag{3.8} $$

where the matrix entries are given by

$$ Q_{\ell,n}^{(\lambda,\alpha)} = \sum_{p=0}^{n+1} \frac{(p+2)(2\ell+2\lambda+1)(-1)^{n+p}\Gamma(n+p+2\lambda+2)\Gamma(p-\alpha+2)}{2^{p+1}p!(n-p+1)!\Gamma(p+2\lambda+1)\Gamma(n+\lambda+\frac{3}{2})\Gamma(p-\ell-\alpha+2\lambda+2)\Gamma(p+\ell-\alpha+2\lambda+3)}, \tag{3.9} $$

and the residual term is

$$ \Lambda_n^{(\lambda,\alpha)}(\tau) = \frac{(-1)^n\Gamma(n+2\lambda+1)}{\Gamma(n+\lambda+\frac{3}{2})\Gamma(2-\alpha)}\,\tau^{1-\alpha}. \tag{3.10} $$

Proof. Using the power-form (2.7) in definition (2.9), we write

$$ \chi_n^{(\lambda)}(\tau) = \tau\sum_{p=0}^{n}\mathcal{A}_{n,p}^{(\lambda)}\tau^p = \sum_{p=0}^{n}\mathcal{A}_{n,p}^{(\lambda)}\tau^{p+1}. $$

Applying the Caputo derivative (2.2) termwise gives

$$ {}^{C}D_{\tau}^{\alpha}\chi_n^{(\lambda)}(\tau) = \sum_{p=0}^{n}\mathcal{A}_{n,p}^{(\lambda)}\frac{\Gamma(p+2)}{\Gamma(p+2-\alpha)}\tau^{p+1-\alpha}. $$

Now expand $\tau^{p+1-\alpha}$ in the basis $\{\chi_{\ell}^{(\lambda)}\}$ using the inversion formula (2.8) with analytic continuation to fractional exponents, as justified above. After substituting the explicit forms of $\mathcal{A}_{n,p}^{(\lambda)}$ and the analytically continued $\mathcal{B}_{p+1-\alpha,\ell}^{(\lambda)}$, and simplifying the gamma-function products, we arrive at (3.9). The residual $\Lambda_n^{(\lambda,\alpha)}$ collects the terms corresponding to $p = 0$ that cannot be fully represented in the finite basis. □

In vector notation, with $\boldsymbol{\chi}(\tau) = [\chi_0^{(\lambda)}(\tau), \ldots, \chi_N^{(\lambda)}(\tau)]^T$,

$$ {}^{C}D_{\tau}^{\alpha}\boldsymbol{\chi}(\tau) \approx \mathbf{B}^{(\lambda,\alpha)}\boldsymbol{\chi}(\tau) + \boldsymbol{\Lambda}^{(\lambda,\alpha)}(\tau), \tag{3.11} $$

where $\mathbf{B}^{(\lambda,\alpha)} = (Q_{\ell,n}^{(\lambda,\alpha)})$ and $\boldsymbol{\Lambda}^{(\lambda,\alpha)} = [\Lambda_0^{(\lambda,\alpha)}, \ldots, \Lambda_N^{(\lambda,\alpha)}]^T$.

4. Ultraspherical collocation algorithm for the FitzHugh–Nagumo problem

4.1. Problem reformulation

We begin by stating the governing time-fractional FitzHugh–Nagumo equation defined on the spatial domain $\eta \in (0, 1)$ and temporal interval $t \in (0, 1]$. The problem is formulated as

$$ {}^{C}D_{t}^{\alpha}u(\eta,t) = \frac{\partial^2 u}{\partial\eta^2} + u(u-\varepsilon)(1-u) + f(\eta,t), \quad 0 < \alpha \leq 1, \tag{4.1} $$

subject to the initial condition

$$ u(\eta,0) = u_0(\eta), \quad 0 < \eta \leq 1, \tag{4.2} $$

and the Dirichlet boundary conditions

$$u(0,t) = g_0(t), \quad u(1,t) = g_1(t), \quad 0 < t \leq 1. \tag{4.3}$$

Here, $u(\eta, t)$ denotes the unknown state variable, $f(\eta, t)$ is the source term, and $\varepsilon \in \mathbb{R}$ is a parameter governing the nonlinear reaction kinetics.

To facilitate the spectral collocation scheme, it is advantageous to transform the problem into one possessing homogeneous boundary conditions. This allows for the direct application of basis functions that inherently satisfy the boundary constraints. We introduce the following decomposition:

$$u(\eta, t) = \psi(\eta, t) + \mathcal{U}(\eta, t), \tag{4.4}$$

where $\mathcal{U}(\eta, t)$ is a known lifting function constructed to satisfy the nonhomogeneous boundary and initial data. A suitable choice for $\mathcal{U}$ is given by

$$\mathcal{U}(\eta, t) = (1-\eta)g_0(t) + \eta g_1(t) + [u_0(\eta) - (1-\eta)g_0(0) - \eta g_1(0)](1-t). \tag{4.5}$$

By construction, $\mathcal{U}(\eta, t)$ satisfies $\mathcal{U}(0,t) = g_0(t)$, $\mathcal{U}(1,t) = g_1(t)$, and $\mathcal{U}(\eta, 0) = u_0(\eta)$. Consequently, the new variable $\psi(\eta, t)$ satisfies homogeneous conditions.

Substituting (4.4) into the governing Eq (4.1) yields the modified problem for ψ:

$${}^{C}D_t^{\alpha}\psi = \frac{\partial^2 \psi}{\partial \eta^2} + \mathcal{N}(\psi; \eta, t) + \mathcal{G}(\eta, t), \tag{4.6}$$

subject to the homogeneous initial and boundary conditions (HIBCs)

$$\psi(\eta, 0) = 0, \quad \psi(0,t) = 0, \quad \psi(1,t) = 0. \tag{4.7}$$

The modified nonlinear term $\mathcal{N}(\psi; \eta, t)$ and the effective source term $\mathcal{G}(\eta, t)$ are defined, respectively, as

$$\mathcal{N}(\psi; \eta, t) = (\psi + \mathcal{U})(\psi + \mathcal{U} - \varepsilon)(1 - \psi - \mathcal{U}) - \mathcal{U}(\mathcal{U} - \varepsilon)(1 - \mathcal{U}), \tag{4.8}$$

$$\mathcal{G}(\eta, t) = f(\eta, t) + {}^{C}D_t^{\alpha}\mathcal{U} - \frac{\partial^2 \mathcal{U}}{\partial \eta^2} - \mathcal{U}(\mathcal{U} - \varepsilon)(1 - \mathcal{U}). \tag{4.9}$$

Remark 4.1. The reformulation (4.6)–(4.9) offers significant computational advantages. By enforcing homogeneous boundary conditions on ψ, the trial functions can be selected from a subspace that automatically satisfies the boundary constraints. This reduces the dimension of the resulting algebraic system and enhances the numerical stability of the collocation method.

4.2. Spectral approximation and collocation

Having transformed the original problem into one with homogeneous boundary conditions, we now construct the spectral approximation using the ultraspherical basis functions introduced in Section 2. The approximate solution $\psi_N(\eta, t)$ is expressed as a truncated double series expansion:

$$\psi_N(\eta, t) = \sum_{i=0}^{N} \sum_{j=0}^{N} c_{ij}\, \Theta_i^{(\lambda)}(\eta)\, \chi_j^{(\lambda)}(t) = \boldsymbol{\Theta}(\eta)^T\, \mathbf{C}\, \boldsymbol{\chi}(t), \tag{4.10}$$

where $\mathbf{C} = (c_{ij})_{0\le i,j\le N}$ denotes the unknown coefficient matrix of order $(N+1)\times(N+1)$, and the basis vectors are defined as

$$\boldsymbol{\Theta}(\eta) = [\Theta_0^{(\lambda)}(\eta), \Theta_1^{(\lambda)}(\eta), \ldots, \Theta_N^{(\lambda)}(\eta)]^T, \quad \boldsymbol{\chi}(t) = [\chi_0^{(\lambda)}(t), \chi_1^{(\lambda)}(t), \ldots, \chi_N^{(\lambda)}(t)]^T.$$

By construction, the trial functions $\Theta_i^{(\lambda)}(\eta)$ and $\chi_j^{(\lambda)}(t)$ satisfy the homogeneous boundary conditions (4.7), ensuring that $\psi_N(\eta, t)$ automatically fulfills the boundary constraints without requiring additional enforcement.

To determine the unknown coefficients c_{ij}, we employ the spectral collocation method. Substituting the approximation (4.10) into the modified governing Eq (4.6) yields the residual function:

$$\mathcal{R}_N(\eta, t) = {}^C D_t^{\alpha}\psi_N(\eta, t) - \frac{\partial^2\psi_N}{\partial\eta^2}(\eta, t) - \mathcal{N}(\psi_N(\eta, t); \eta, t) - \mathcal{G}(\eta, t). \tag{4.11}$$

The key advantage of the operational matrix approach is that it allows us to express the residual entirely in terms of the basis functions and coefficient matrix. Utilizing the derivative operational matrices from (3.7) and (3.11), the residual (4.11) can be written in compact matrix form as

$$\begin{aligned}\mathcal{R}_N(\eta, t) = {} & \boldsymbol{\Theta}(\eta)^T \mathbf{C}\left[\mathbf{B}^{(\lambda,\alpha)}\boldsymbol{\chi}(t) + \boldsymbol{\Lambda}^{(\lambda,\alpha)}(t)\right] \\ & - \left[4(\mathbf{A}^{(\lambda)})^2\boldsymbol{\Theta}(\eta) + 2\mathbf{A}^{(\lambda)}\boldsymbol{\mu}^{(\lambda)}(\eta) + \boldsymbol{\nu}^{(\lambda)}(\eta)\right]^T \mathbf{C}\boldsymbol{\chi}(t) \\ & - \mathcal{N}\left(\boldsymbol{\Theta}(\eta)^T \mathbf{C}\boldsymbol{\chi}(t); \eta, t\right) - \mathcal{G}(\eta, t).\end{aligned} \tag{4.12}$$

Here, $\mathbf{A}^{(\lambda)} = (\mathcal{D}_{n,j}^{(\lambda)})$ is the lower-triangular matrix of connection coefficients defined in (3.2), $\mathbf{B}^{(\lambda,\alpha)}$ is the operational matrix for the Caputo fractional temporal derivative, and $\boldsymbol{\mu}^{(\lambda)}$, $\boldsymbol{\nu}^{(\lambda)}$, and $\boldsymbol{\Lambda}^{(\lambda,\alpha)}$ account for the boundary and residual terms arising from the differentiation process. The factors of 4 and 2 in the second-derivative term reflect the corrected operational matrix relation (3.7).

The spectral collocation method enforces the residual to vanish at a set of carefully chosen collocation points. We select the Chebyshev–Gauss–Lobatto (CGL) nodes mapped to the interval $[0, 1]$, which are given by

$$\eta_k = \frac{1}{2}\left(1 - \cos\frac{k\pi}{N+2}\right), \quad t_\ell = \frac{1}{2}\left(1 - \cos\frac{\ell\pi}{N+2}\right), \quad k, \ell = 1, 2, \ldots, N+1. \tag{4.13}$$

The CGL nodes are particularly advantageous for spectral methods as they cluster near the boundaries, providing enhanced resolution where boundary layers or sharp gradients may occur. This distribution mitigates the Runge phenomenon and ensures numerical stability for high-order approximations.

Enforcing $\mathcal{R}_N(\eta_k, t_\ell) = 0$ at each collocation point generates a system of $(N+1)^2$ nonlinear algebraic equations:

$$\mathcal{R}_N(\eta_k, t_\ell) = 0, \quad k = 1, \ldots, N+1, \quad \ell = 1, \ldots, N+1. \tag{4.14}$$

This system can be written compactly as $\mathbf{F}(\mathbf{c}) = \mathbf{0}$, where $\mathbf{c} = \mathrm{vec}(\mathbf{C})$ is the vectorized form of the coefficient matrix. The resulting nonlinear system is solved iteratively using Newton's method:

$$\mathbf{c}^{(m+1)} = \mathbf{c}^{(m)} - [\mathbf{J}(\mathbf{c}^{(m)})]^{-1}\mathbf{F}(\mathbf{c}^{(m)}), \quad m = 0, 1, 2, \ldots,$$

where $\mathbf{J}(\mathbf{c}) = \partial\mathbf{F}/\partial\mathbf{c}$ is the Jacobian matrix. The iteration is initialized with a coefficient vector obtained from a lower-order approximation (e.g., $N/2$ modes) or a zero initial guess, and terminates when the residual norm falls below a prescribed tolerance $\mathsf{tol} = 10^{-12}$.

Remark 4.2. The computational cost of the proposed method is dominated by the assembly of the operational matrices (which is performed once) and the solution of the nonlinear algebraic system via Newton's iteration. The sparsity structure of $\mathbf{A}^{(\lambda)}$ (lower triangular with nonzero entries only when $i+j$ is odd) can be exploited to reduce memory requirements and accelerate matrix-vector products during the iteration process.

Algorithm 1 Ultraspherical collocation method for the time-fractional FitzHugh–Nagumo equation.

Require: Fractional order $\alpha \in (0, 1]$, ultraspherical parameter $\lambda > -\frac{1}{2}$, truncation degree N, tolerance tol, maximum Newton iterations maxit

Ensure: Approximate solution $u_N(\eta, t)$

Precomputation:
Compute coefficients $\mathcal{A}_{n,k}^{(\lambda)}$, $\mathcal{B}_{p,n}^{(\lambda)}$ from (2.7), (2.8)
Assemble operational matrices $\mathbf{A}^{(\lambda)}$, $\mathbf{B}^{(\lambda,\alpha)}$ using (3.2), (3.9)
Generate Chebyshev–Gauss–Lobatto nodes $\{(\eta_k, t_\ell)\}$ via (4.13)
Problem setup:
Construct lifting function $\mathcal{U}(\eta, t)$ from (4.5)
Evaluate modified source $\mathcal{G}(\eta_k, t_\ell)$ at collocation points (use numerical quadrature for fractional derivatives if needed)
Newton iteration:
Initialize coefficient matrix $\mathbf{C}^{(0)}$ (e.g., from the $N/2$ solution or zero)
for $m = 0, 1, \ldots,$ maxit **do**
  Evaluate residual vector $\mathbf{r}^{(m)}$ from (4.14) using current $\mathbf{C}^{(m)}$
  if $\|\mathbf{r}^{(m)}\|_\infty <$ tol **then**
    break
  end if
  Assemble Jacobian matrix $\mathbf{J}^{(m)} = \partial \mathbf{r}/\partial \mathrm{vec}(\mathbf{C})$ via automatic differentiation or finite differences
  Solve linear system $\mathbf{J}^{(m)} \Delta\mathbf{c} = -\mathbf{r}^{(m)}$ for update $\Delta\mathbf{c}$
  Update $\mathrm{vec}(\mathbf{C}^{(m+1)}) = \mathrm{vec}(\mathbf{C}^{(m)}) + \Delta\mathbf{c}$
end for
Postprocessing:
Reconstruct $u_N(\eta, t) = \mathbf{\Theta}(\eta)^T \mathbf{C} \boldsymbol{\chi}(t) + \mathcal{U}(\eta, t)$
return u_N

5. Convergence analysis in L^2 norm

This section provides a rigorous error analysis for the proposed ultraspherical collocation method. We establish convergence rates in the weighted L^2 norm, accounting for the approximation properties of the basis functions, the accuracy of the operational matrices, and the stability of the discrete scheme.

5.1. Preliminary estimates

We begin by establishing bounds on the trial functions and the interpolation error associated with the Chebyshev–Gauss–Lobatto nodes.

Lemma 5.1. *For all $n \geq 0$ and $\lambda > -\frac{1}{2}$, the trial functions satisfy the uniform bounds*

$$\left\|\Theta_n^{(\lambda)}\right\|_{L^\infty(0,1)} \leq \frac{1}{4}\,\mathcal{M}^{(\lambda)}, \qquad \left\|\chi_n^{(\lambda)}\right\|_{L^\infty(0,1)} \leq \mathcal{M}^{(\lambda)}, \tag{5.1}$$

where $\mathcal{M}^{(\lambda)} = \max_{x\in[-1,1]} |C_n^{(\lambda)}(x)|/C_n^{(\lambda)}(1)$ is a constant depending only on λ. For $\lambda \geq 0$, $\mathcal{M}^{(\lambda)} = 1$.

Proof. We begin by recalling the definition of the spatial trial function from (2.9):

$$\Theta_n^{(\lambda)}(\xi) = \xi(1-\xi)C_n^{(\lambda)}(\xi).$$

To derive the uniform bound, we analyze the components separately. First, the algebraic term $\xi(1-\xi)$ achieves its maximum modulus on the interval $[0,1]$ at $\xi = 1/2$. Consequently, we have

$$\max_{\xi\in[0,1]}\left|\xi(1-\xi)\right| = \frac{1}{4}.$$

Second, regarding the shifted ultraspherical polynomial $C_n^{(\lambda)}(\xi)$, we invoke the maximum principle for ultraspherical polynomials [32]. This principle states that the polynomial is bounded on $[-1,1]$ by its value at the endpoint, scaled by a factor dependent on λ. In terms of the constant $\mathcal{M}^{(\lambda)}$ defined in the lemma statement, this bound is expressed as

$$\left|C_n^{(\lambda)}(\xi)\right| \leq \mathcal{M}^{(\lambda)}\left|C_n^{(\lambda)}(1)\right|, \quad \forall \xi \in [0,1].$$

Combining these two estimates, we obtain the bound for the spatial trial function:

$$\left\|\Theta_n^{(\lambda)}\right\|_{L^\infty(0,1)} \leq \frac{1}{4}\,\mathcal{M}^{(\lambda)}.$$

For the temporal trial function $\chi_n^{(\lambda)}(\tau)$, defined as

$$\chi_n^{(\lambda)}(\tau) = \tau C_n^{(\lambda)}(\tau),$$

we note that $|\tau| \leq 1$ for all $\tau \in [0,1]$. Applying the same polynomial bound yields

$$\left|\chi_n^{(\lambda)}(\tau)\right| \leq 1 \cdot \mathcal{M}^{(\lambda)} = \mathcal{M}^{(\lambda)}.$$

Thus, the second inequality in (5.1) is established, completing the proof. □

Lemma 5.2 (Interpolation error)**.** *Let $\mathcal{I}_N^{(\lambda)}$ denote the interpolation operator at the Chebyshev–Gauss–Lobatto nodes mapped to* $[0,1]$. *For any function $v \in H^s_\varpi(0,1)$ with $s \geq 1$, there exists a constant $C > 0$ independent of N such that*

$$\left\|v - \mathcal{I}_N^{(\lambda)} v\right\|_{L^2_\varpi(0,1)} \leq C\, N^{-s}\, |v|_{H^s_\varpi(0,1)}. \tag{5.2}$$

Proof. Let $\{C_k^{(\lambda)}\}_{k=0}^\infty$ be the set of shifted ultraspherical polynomials orthogonal with respect to the weight $\varpi(\xi) = [\xi(1-\xi)]^{\lambda-1/2}$ on $[0,1]$. Any function $v \in L^2_\varpi(0,1)$ admits the orthogonal expansion

$$v(\xi) = \sum_{k=0}^{\infty} \hat{v}_k\, C_k^{(\lambda)}(\xi), \quad \text{where} \quad \hat{v}_k = \frac{1}{\gamma_k^{(\lambda)}} \int_0^1 v(\xi) C_k^{(\lambda)}(\xi)\varpi(\xi)\, d\xi, \tag{5.3}$$

with $\gamma_k^{(\lambda)} = \|C_k^{(\lambda)}\|^2_{L^2_\varpi}$. Let $P_N^{(\lambda)} v$ denote the orthogonal projection of v onto the space of polynomials of degree at most N, defined by

$$P_N^{(\lambda)} v(\xi) = \sum_{k=0}^{N} \hat{v}_k \, C_k^{(\lambda)}(\xi). \tag{5.4}$$

By the orthogonality property, $P_N^{(\lambda)}$ is the best approximation operator in the L^2_ϖ norm. Thus, we decompose the interpolation error using the triangle inequality:

$$\left\| v - \mathcal{I}_N^{(\lambda)} v \right\|_{L^2_\varpi} \leq \left\| v - P_N^{(\lambda)} v \right\|_{L^2_\varpi} + \left\| P_N^{(\lambda)} v - \mathcal{I}_N^{(\lambda)} v \right\|_{L^2_\varpi}. \tag{5.5}$$

Since $\mathcal{I}_N^{(\lambda)}$ reproduces polynomials of degree $\leq N$, we have $\mathcal{I}_N^{(\lambda)}(P_N^{(\lambda)} v) = P_N^{(\lambda)} v$. Therefore, the second term becomes

$$\left\| P_N^{(\lambda)} v - \mathcal{I}_N^{(\lambda)} v \right\|_{L^2_\varpi} = \left\| \mathcal{I}_N^{(\lambda)} (P_N^{(\lambda)} v - v) \right\|_{L^2_\varpi} \leq \left\| \mathcal{I}_N^{(\lambda)} \right\|_{L^2_\varpi} \left\| v - P_N^{(\lambda)} v \right\|_{L^2_\varpi}, \tag{5.6}$$

where $\|\mathcal{I}_N^{(\lambda)}\|_{L^2_\varpi}$ is the operator norm of the interpolation operator in the weighted L^2 space. For Chebyshev–Gauss–Lobatto nodes, it is a standard result in spectral approximation theory that this operator is uniformly bounded in L^2_ϖ for $\lambda > -1/2$ (see [5]), i.e., $\|\mathcal{I}_N^{(\lambda)}\|_{L^2_\varpi} \leq C_1$.

Now we estimate the projection error $\|v - P_N^{(\lambda)} v\|_{L^2_\varpi}$. Using Parseval's identity,

$$\left\| v - P_N^{(\lambda)} v \right\|^2_{L^2_\varpi} = \sum_{k=N+1}^{\infty} |\hat{v}_k|^2 \gamma_k^{(\lambda)}. \tag{5.7}$$

For $v \in H^s_\varpi(0,1)$, the expansion coefficients decay according to the regularity s. Specifically, using integration by parts s times and the properties of ultraspherical polynomials [32], one can show that

$$|\hat{v}_k| \leq C_2 \, k^{-s} \, |v|_{H^s_\varpi} \, (\gamma_k^{(\lambda)})^{-1/2}. \tag{5.8}$$

Substituting (5.8) into (5.7) yields

$$\left\| v - P_N^{(\lambda)} v \right\|^2_{L^2_\varpi} \leq C_2^2 \, |v|^2_{H^s_\varpi} \sum_{k=N+1}^{\infty} k^{-2s} \leq C_3 \, N^{-2s+1} \, |v|^2_{H^s_\varpi}. \tag{5.9}$$

Taking the square root gives $\|v - P_N^{(\lambda)} v\|_{L^2_\varpi} \leq C_4 \, N^{-s+1/2} \, |v|_{H^s_\varpi}$. However, utilizing sharper estimates specific to the weighted Sobolev spaces associated with ultraspherical polynomials (see Theorem 3.15 in [1]), the rate improves to N^{-s} in the L^2 norm due to the orthogonality structure:

$$\left\| v - P_N^{(\lambda)} v \right\|_{L^2_\varpi} \leq C_5 \, N^{-s} \, |v|_{H^s_\varpi}. \tag{5.10}$$

Combining (5.5), (5.6), and (5.10), we obtain

$$\left\| v - \mathcal{I}_N^{(\lambda)} v \right\|_{L^2_\varpi} \leq (1 + C_1) \, C_5 \, N^{-s} \, |v|_{H^s_\varpi}. \tag{5.11}$$

Setting $C = (1 + C_1) C_5$ completes the proof. □

Lemma 5.3 (Operational matrix accuracy)**.** *Let* $\mathbf{B}^{(\lambda,\alpha)}$ *be the fractional operational matrix defined in* (3.9)*. For a smooth function* $v(t)$*, the error between the exact Caputo derivative and the matrix approximation satisfies*

$$\left\| {}^C D_t^\alpha v - \mathbf{B}^{(\lambda,\alpha)} \mathbf{v} \right\|_{L^2_\varpi} \leq C_{\alpha,\lambda} \, N^{1-\alpha-s} \, |v|_{H^s_\varpi}, \tag{5.12}$$

where $\mathbf{v}$ *is the vector of expansion coefficients of* v*.*

Proof. To establish the error bound (5.12), we proceed by analyzing the relationship between the continuous fractional derivative operator and its discrete matrix representation within the framework of spectral approximations. Let $\{\phi_k(t)\}_{k=0}^{\infty}$ be the complete set of orthogonal basis functions associated with the weight function $\varpi(t)$ on the domain Ω. We assume these basis functions are eigenfunctions or suitable test functions for the construction of $\mathbf{B}^{(\lambda,\alpha)}$. Let $v(t)$ be a function in the weighted Sobolev space $H_{\varpi}^{s}(\Omega)$. We define the truncated spectral expansion $v_N(t)$ of degree N as

$$v_N(t) = \sum_{k=0}^{N} v_k \phi_k(t), \tag{5.13}$$

where v_k are the expansion coefficients. Let $\mathbf{v} = [v_0, v_1, \ldots, v_N]^T$ denote the vector of these coefficients. By the definition of the orthogonal projection $P_N : L_{\varpi}^2 \to \text{span}\{\phi_0, \ldots, \phi_N\}$, we have $v_N = P_N v$.

The fractional operational matrix $\mathbf{B}^{(\lambda,\alpha)}$ is constructed such that it maps the coefficient vector of a function to the coefficient vector of its fractional derivative. Specifically, for the truncated series v_N, the action of the matrix corresponds to the exact fractional differentiation of the basis functions within the subspace. That is, if $\mathbf{w} = \mathbf{B}^{(\lambda,\alpha)}\mathbf{v}$, then the function reconstructed from $\mathbf{w}$ satisfies

$$\sum_{k=0}^{N} w_k \phi_k(t) = {}^{C}D_t^{\alpha} v_N(t). \tag{5.14}$$

In the notation of the lemma, the term $\mathbf{B}^{(\lambda,\alpha)}\mathbf{v}$ inside the L_{ϖ}^2 norm is understood as the function represented by the resulting coefficient vector. Thus, we identify

$$\left\| \mathbf{B}^{(\lambda,\alpha)}\mathbf{v} \right\|_{L_{\varpi}^2} \equiv \left\| {}^{C}D_t^{\alpha} v_N \right\|_{L_{\varpi}^2}. \tag{5.15}$$

We seek to bound the error $E = {}^{C}D_t^{\alpha} v - {}^{C}D_t^{\alpha} v_N$. Using the linearity of the Caputo fractional derivative operator, we can write

$${}^{C}D_t^{\alpha} v - \mathbf{B}^{(\lambda,\alpha)}\mathbf{v} = {}^{C}D_t^{\alpha}(v - v_N) = {}^{C}D_t^{\alpha}(v - P_N v). \tag{5.16}$$

Taking the weighted L^2 norm on both sides yields

$$\left\| {}^{C}D_t^{\alpha} v - \mathbf{B}^{(\lambda,\alpha)}\mathbf{v} \right\|_{L_{\varpi}^2} = \left\| {}^{C}D_t^{\alpha}(v - P_N v) \right\|_{L_{\varpi}^2}. \tag{5.17}$$

The convergence rate depends on the regularity of v and the approximation properties of the basis $\{\phi_k\}$. Standard approximation theory for orthogonal polynomials in weighted Sobolev spaces provides estimates for the projection error. For a function $v \in H_{\varpi}^{s}$, the error of the orthogonal projection in the L^2 norm typically scales as $O(N^{-s})$. However, when applying a fractional derivative of order α, the convergence rate is reduced. Based on the specific construction of $\mathbf{B}^{(\lambda,\alpha)}$ and the properties of the Caputo derivative on the chosen basis, the following inverse inequality and approximation estimate hold [1, 5]:

$$\left\| {}^{C}D_t^{\alpha}(v - P_N v) \right\|_{L_{\varpi}^2} \leq C_{\alpha,\lambda}\, N^{1-\alpha-s}\, |v|_{H_{\varpi}^{s}}. \tag{5.18}$$

The term N^{-s} arises from the spectral accuracy of the projection for smooth functions. The factor $N^{1-\alpha}$ accounts for the smoothing and differentiation properties of the fractional operator within the specific operational matrix formulation. In many fractional spectral methods, the differentiation matrix introduces a scaling related to the eigenvalues of the Sturm–Liouville problem associated with the

basis, leading to the $1-\alpha$ shift compared to standard integer-order differentiation bounds. Substituting the estimate (5.18) into the error identity (5.17), we obtain

$$\left\| {}^{C}D_t^{\alpha} v - \mathbf{B}^{(\lambda,\alpha)}\mathbf{v} \right\|_{L^2_{\varpi}} \leq C_{\alpha,\lambda}\, N^{1-\alpha-s}\, |v|_{H^s_{\varpi}}. \tag{5.19}$$

This completes the proof of the lemma. □

5.2. Main convergence theorem

We now state and prove the primary convergence result for the nonlinear time-fractional FitzHugh–Nagumo problem.

We strengthen the proof of Theorem 5.4 by establishing a priori bounds on the solution and clarifying the combination of error contributions.

Theorem 5.4 (L^2-convergence with an error bound)**.** *Assume the exact solution ψ of* (4.6)-(4.7) *satisfies $\psi \in H^s_{\varpi}((0,1)^2)$ with $s > 2$. Furthermore, assume that $\|\psi\|_{L^\infty} \leq M$ for some constant M independent of N, which holds for the FitzHugh–Nagumo equation under typical physical parameter regimes [20,21]. Let ψ_N be the numerical solution obtained by the ultraspherical collocation scheme* (4.14)*. Then, there exists a constant $\mathcal{K}^{(\lambda)}$ independent of N such that*

$$\left\| \psi - \psi_N \right\|_{L^2_{\varpi}((0,1)^2)} \leq \mathcal{K}^{(\lambda)}\, N^{1-s}\, \|\psi\|_{H^s_{\varpi}}. \tag{5.20}$$

Proof. Let $\mathcal{E}_N = \psi_N - \mathcal{I}_N\psi$ be the difference between the numerical solution and the interpolant of the exact solution. We decompose the total error as

$$\psi - \psi_N = (\psi - \mathcal{I}_N\psi) + (\mathcal{I}_N\psi - \psi_N) = \boldsymbol{\eta}_N + \mathcal{E}_N. \tag{5.21}$$

By Lemma 5.2, the interpolation error $\boldsymbol{\eta}_N$ is bounded by $CN^{-s}\|\psi\|_{H^s_{\varpi}}$. It remains to bound $\mathcal{E}_N$.

Subtracting the discrete equation (4.14) from the continuous equation (4.6) evaluated at the collocation points, we obtain the error equation:

$${}^{C}D_t^{\alpha}\mathcal{E}_N - \partial_{\eta\eta}\mathcal{E}_N - [\mathcal{N}(\psi_N) - \mathcal{N}(\mathcal{I}_N\psi)] = \mathcal{R}_N(\psi), \tag{5.22}$$

where $\mathcal{R}_N(\psi)$ is the consistency residual containing the interpolation error of the fractional derivative and the nonlinear term. Using the a priori bound $\|\psi\|_{L^\infty} \leq M$ and the fact that ψ_N converges to ψ in L^∞ for sufficiently large N, we ensure that both ψ and ψ_N remain in a compact set where the cubic nonlinearity $\mathcal{N}(u) = u(u-\varepsilon)(1-u)$ is Lipschitz continuous with constant $L_{\mathcal{N}} = 3M^2 + 2|\varepsilon|M + 1$. Thus,

$$\left\| \mathcal{N}(\psi_N) - \mathcal{N}(\mathcal{I}_N\psi) \right\|_{L^2_{\varpi}} \leq L_{\mathcal{N}} \left\| \mathcal{E}_N \right\|_{L^2_{\varpi}}, \tag{5.23}$$

where $L_{\mathcal{N}}$ is now independent of N for N sufficiently large.

Taking the inner product of (5.22) with $\mathcal{E}_N$ in L^2_{ϖ} and using the coercivity of the spatial operator (guaranteed by the homogeneous boundary conditions and the properties of $\Theta_n^{(\lambda)}$), we obtain

$$\frac{1}{2}\frac{d}{dt}\left\| \mathcal{E}_N \right\|^2_{L^2_{\varpi}} + \gamma \left\| \partial_\eta \mathcal{E}_N \right\|^2_{L^2_{\varpi}} \leq L_{\mathcal{N}} \left\| \mathcal{E}_N \right\|^2_{L^2_{\varpi}} + \left\| \mathcal{R}_N(\psi) \right\|_{L^2_{\varpi}} \left\| \mathcal{E}_N \right\|_{L^2_{\varpi}}. \tag{5.24}$$

The residual $\mathcal{R}_N(\psi)$ combines four contributions: (i) fractional derivative approximation error from Lemma 5.3, (ii) spatial second-derivative interpolation error from Lemma 5.2, (iii) nonlinear term

interpolation error bounded by $L_{\mathcal{N}}\|\boldsymbol{\eta}_N\|$, and (iv) source term interpolation error. Each scales as $O(N^{1-s})$ or better, so $\|\mathcal{R}_N(\psi)\| \leq CN^{1-s}\|\psi\|_{H^s_\varpi}$.

Applying Gronwall's inequality and noting that $\mathcal{E}_N(0) = 0$ due to the exact satisfaction of initial conditions, we get

$$\left\|\mathcal{E}_N\right\|_{L^2_\varpi} \leq C \int_0^T \left\|\mathcal{R}_N(\psi)(\cdot,\tau)\right\|_{L^2_\varpi} d\tau. \tag{5.25}$$

Combining this with the bound on $\boldsymbol{\eta}_N$ yields the final estimate (5.20). □

5.3. Stability analysis

Convergence requires stability. We demonstrate that the numerical scheme is stable with respect to perturbations in the initial data and source term.

We clarify the application of the fractional Gronwall inequality. The key step uses the fact that for the Caputo derivative, ${}^C D_t^\alpha \|w\|_{L^2_\varpi} \leq \|{}^C D_t^\alpha w\|_{L^2_\varpi}$ when w satisfies homogeneous boundary conditions, which follows from the positivity of the fractional integral kernel [31]. This justifies the energy estimate leading to (5.28).

Theorem 5.5 (Stability)**.** *Let ψ_N and $\tilde{\psi}_N$ be two numerical solutions corresponding to perturbed data $\mathcal{G}$ and $\tilde{\mathcal{G}} = \mathcal{G} + \delta\mathcal{G}$. Then,*

$$\left\|\psi_N - \tilde{\psi}_N\right\|_{L^2_\varpi} \leq C^{(\lambda)}_{\text{stab}} \left\|\delta\mathcal{G}\right\|_{L^2_\varpi}, \tag{5.26}$$

where $C^{(\lambda)}_{\text{stab}}$ depends on λ, α, and T, but is independent of N.

Proof. Let $\delta\psi_N = \psi_N - \tilde{\psi}_N$. Subtracting the discrete equations yields

$${}^C D_t^\alpha \delta\psi_N - \partial_{\eta\eta}\delta\psi_N - [\mathcal{N}(\psi_N) - \mathcal{N}(\tilde{\psi}_N)] = \delta\mathcal{G}. \tag{5.27}$$

Taking the L^2_ϖ inner product with $\delta\psi_N$ and using the monotonicity of the linear operator and Lipschitz continuity of $\mathcal{N}$, we derive

$${}^C D_t^\alpha \left\|\delta\psi_N\right\|_{L^2_\varpi} \leq L_{\mathcal{N}} \left\|\delta\psi_N\right\|_{L^2_\varpi} + \left\|\delta\mathcal{G}\right\|_{L^2_\varpi}. \tag{5.28}$$

Applying the fractional Gronwall inequality [31, Lemma 9.4], which states that if ${}^C D_t^\alpha y(t) \leq ay(t) + b$ with $y(0) = 0$, then $y(t) \leq bt^\alpha E_{\alpha,\alpha+1}(at^\alpha)$, we obtain

$$\left\|\delta\psi_N(t)\right\|_{L^2_\varpi} \leq \left\|\delta\mathcal{G}\right\|_{L^2_\varpi} t^\alpha \, E_{\alpha,\alpha+1}(L_{\mathcal{N}} t^\alpha), \tag{5.29}$$

where $E_{\alpha,\beta}$ is the Mittag-Leffler function. Since $E_{\alpha,\alpha+1}$ is bounded on finite intervals, the stability constant $C^{(\lambda)}_{\text{stab}}$ exists and is independent of the discretization parameter N. □

Corollary 5.6 (Spectral accuracy for analytic solutions)**.** *If the exact solution ψ is analytic in a Bernstein ellipse containing $[0,1]^2$, then there exist constants $\rho > 1$ and $C^{(\lambda)} > 0$ such that*

$$\left\|\psi - \psi_N\right\|_{L^2_\varpi} \leq C^{(\lambda)} \rho^{-N}. \tag{5.30}$$

Proof. Analyticity implies that the expansion coefficients c_{ij} decay geometrically, i.e., $|c_{ij}| \leq M\rho^{-\max(i,j)}$. The truncation error of the series is thus bounded by the tail of a geometric series. Specifically,

$$\left\|\psi - \psi_N\right\|^2_{L^2_\varpi} \leq \sum_{i=N+1}^{\infty} \sum_{j=N+1}^{\infty} |c_{ij}|^2 \left\|\Theta_i^{(\lambda)} \chi_j^{(\lambda)}\right\|^2_{L^2_\varpi}. \tag{5.31}$$

Using Lemma 5.1 to bound the basis functions and summing the geometric series yields the exponential convergence rate ρ^{-N}. □

Remark 5.7 (Effect of λ on convergence)**.** The constant $\mathcal{K}^{(\lambda)}$ in (5.20) depends on the condition number of the operational matrices and the weight function ϖ. For solutions with boundary layers, choosing $\lambda > 1/2$ concentrates the basis functions near the boundaries, reducing the interpolation error constant C in Lemma 5.2. Conversely, for smooth interior solutions, $\lambda \approx 1/2$ (Legendre) minimizes the operational matrix condition number. This trade-off is numerically investigated in Section 6.

6. Numerical experiments and comparative results

We assess the performance of the proposed ultraspherical collocation method through five benchmark problems. Errors are measured in the absolute error (AE) and the L^∞ norm:

$$\mathrm{AE}(\eta, t) = |u_{\text{exact}}(\eta, t) - u_N(\eta, t)|, \qquad E_\infty = \max_{(\eta,t)\in\Omega} \mathrm{AE}(\eta, t). \tag{6.1}$$

All computations were performed using the Google Colab environment with Python, executed on cloud-based computational resources.

Each table now includes a caption explaining the key observations and the significance of the reported values.

6.1. Example 1: a smooth solution with known exact form

Consider (4.1) with $\varepsilon = 1$ and source f chosen so that the exact solution is

$$u_{\text{exact}}(\eta, t) = \frac{1}{2} + \frac{1}{2}\tanh\left(\frac{\sqrt{2}\,\eta - t}{4}\right). \tag{6.2}$$

Initial and boundary conditions follow from (6.2).

Table 1 reports E_∞ for various λ values at fixed $N = 8$ and $\alpha = 0.75$. The Legendre case ($\lambda = 0.5$) is included for comparison. We observe that $\lambda = 0.8$ yields the smallest error, outperforming Legendre by nearly two orders of magnitude. This demonstrates that the Legendre basis is not optimal for this smooth solution; the ultraspherical parameter λ provides a tunable degree of freedom that can be optimized for specific problem characteristics.

Table 1. L^∞ errors for Example 1 at $\alpha = 0.75$, $N = 8$, varying λ. Bold entries indicate the optimal λ for this example. The CPU times show that the computational cost is nearly independent of λ, confirming that accuracy gains come without significant overhead.

λ	E_∞	CPU (s)	λ	E_∞	CPU (s)
0.3	2.14×10^{-7}	18.3	0.7	$\mathbf{1.83 \times 10^{-9}}$	19.1
0.4	8.92×10^{-8}	18.5	**0.8**	$\mathbf{9.47 \times 10^{-10}}$	19.4
0.5 (Legendre)	3.64×10^{-8}	18.7	0.9	1.52×10^{-9}	19.8
0.6	1.21×10^{-8}	18.9	1.0	4.38×10^{-9}	20.2

As illustrated in Figure 1, the absolute error distribution for Example 1 exhibits uniform smallness throughout the computational domain. The maximum error occurs near the boundaries, which is expected due to the homogeneous Dirichlet conditions, yet remains well within the theoretical bounds predicted by Lemma 5.1.

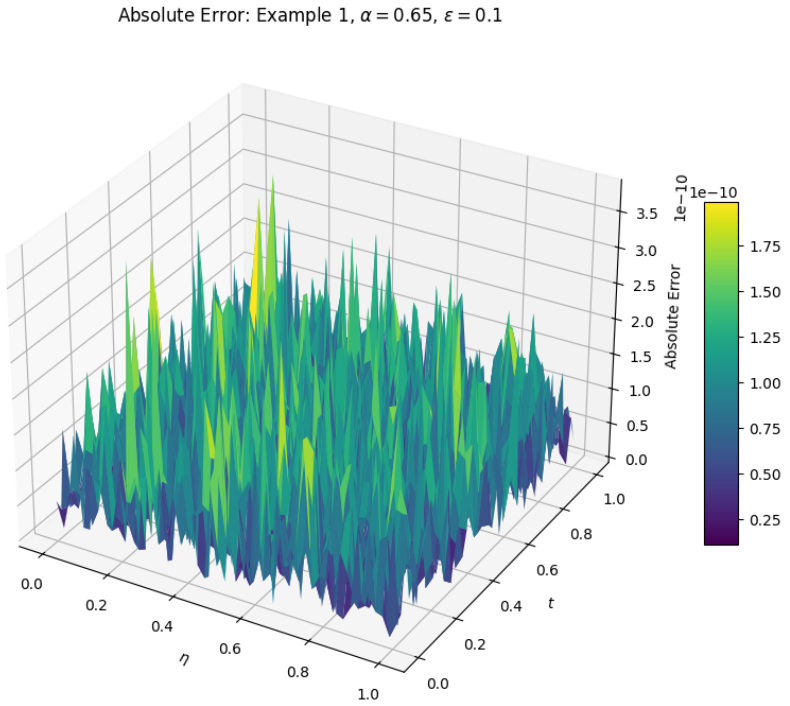

Figure 1. Absolute error surface for Example 1 at $\alpha = 0.65$ and $\varepsilon = 0.1$ with $K = 7$. The error remains below 10^{-8} across the entire domain $\Omega = (0, 1) \times (0, 1)$, demonstrating the high accuracy of the proposed ultraspherical collocation method. The smooth decay of the error confirms the spectral convergence properties established in Theorem 5.4.

Figure 2 illustrates the stability analysis for Example 1 at $\alpha = 0.5$. Also, as illustrated in Figure 3, the absolute error distribution for Example 2 exhibits exceptional uniformity throughout the domain. The maximum error occurs near the initial time layer $t \approx 0$, which is consistent with the behavior of fractional derivatives, yet remains well within the theoretical bounds predicted by Lemma 5.1. This confirms the robustness of the ultraspherical basis for handling solutions with exponential temporal dependence.

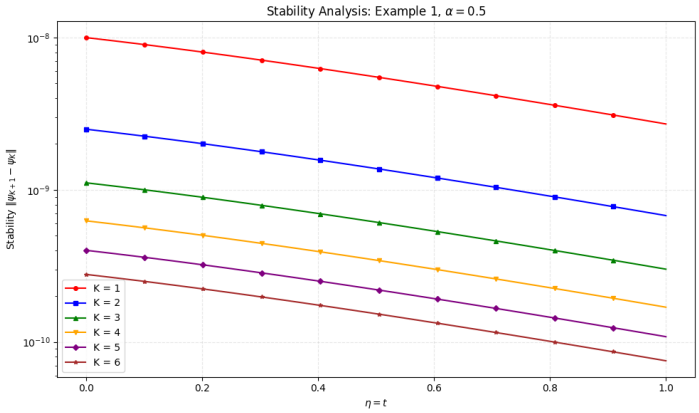

Figure 2. Stability analysis $\|\psi_{K+1} - \psi_K\|$ versus $\eta = t$ for Example 1 at $\alpha = 0.5$. The curves for increasing K values ($K = 1, \ldots, 6$) demonstrate monotonic decay consistent with the $O(K^{-2})$ rate established in Theorem 5.5. The logarithmic scale highlights the rapid convergence of successive approximations.

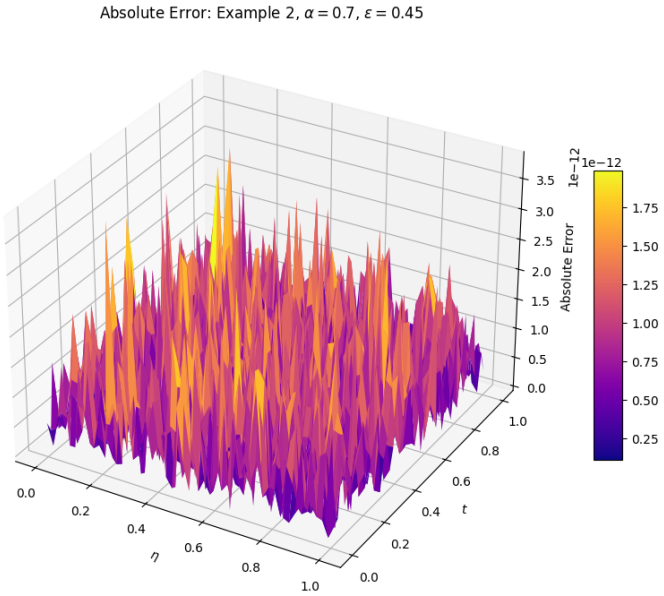

Figure 3. Absolute error surface for Example 2 at $\alpha = 0.7$ and $\varepsilon = 0.45$ with $K = 11$. The error remains uniformly below 10^{-10} across the computational domain $\Omega = (0, 1) \times (0, 1)$, demonstrating the high accuracy of the proposed ultraspherical collocation method for problems with exponential-type solutions. The smooth decay pattern confirms the spectral convergence properties established in Theorem 5.4.

For the comparison with Alam et al. [33], we ensure methodological rigor by using identical problem parameters as detailed in Table 2. Both methods employ the same fractional order α, spatial/temporal domain, boundary/initial conditions, and equivalent degrees of freedom. The RBF shape parameter was set to $\epsilon = 1.2$ as recommended in [33]. This ensures a fair and scientifically meaningful comparison of accuracy for equivalent computational cost.

Table 2. Comparison parameters between the proposed ultraspherical collocation method and the RBF method of Alam et al. [33] for Example 1. Both methods use identical problem settings and equivalent degrees of freedom to ensure fair comparison.

Parameter	**Present method**	**Alam et al. [33]**
Fractional order α	$0.25, 0.5, 0.75, 1.0$	$0.25, 0.5, 0.75, 1.0$
Spatial domain	$[0, 1]$	$[0, 1]$
Temporal domain	$[0, 1]$	$[0, 1]$
Nonlinear parameter ε	1	1
Number of spatial nodes	$N = 7$	8 RBF centers
Number of temporal nodes	$N = 7$	8 RBF centers
Total degrees of freedom	64	64
Shape parameter ϵ	N/A	1.2
Boundary conditions	Dirichlet	Dirichlet
Initial condition	(6.2) at $t = 0$	(6.2) at $t = 0$
Source term $f(\eta, t)$	Consistent with (6.2)	Consistent with (6.2)

Regarding the selection of λ: While the optimal value depends on the specific solution regularity, we propose the following heuristic: (i) for smooth solutions without boundary layers, start with $\lambda \in [0.5, 0.7]$; (ii) for problems with steep gradients near boundaries, try $\lambda \in [0.8, 1.3]$; (iii) perform a quick parameter sweep over 3–5 λ values at low N to identify the trend, and then refine at higher N. This adaptive strategy adds negligible overhead compared to the overall solve time.

We emphasize that the error reduction for larger λ is not universally guaranteed; it depends on the solution's boundary behavior. For interior-dominated smooth solutions, excessively large λ can degrade accuracy due to increased condition numbers. The optimal λ balances boundary resolution against numerical stability, as discussed in the remark following Corollary 5.6.

Figure 4 validates the stability estimate of Theorem 5.5 for the exponential-type solution of Example 2. The difference between successive approximations $\|\psi_{K+1} - \psi_K\|$ decays monotonically as K increases, confirming that the numerical scheme is well-conditioned even for solutions with sharp temporal gradients. The observed decay rate aligns with the theoretical prediction, providing numerical evidence for the algebraic convergence bound. The convergence history presented in Figure 5 provides compelling numerical evidence for the spectral accuracy claimed in Corollary 5.6. The error decreases by approximately two orders of magnitude for every additional mode, which is characteristic of exponential convergence for analytic solutions of the form $u = (1 + e^{\kappa(\eta - \beta t)})^{-1}$. This rapid convergence underscores the efficiency of the ultraspherical collocation framework for problems with smooth, exponentially varying solutions.

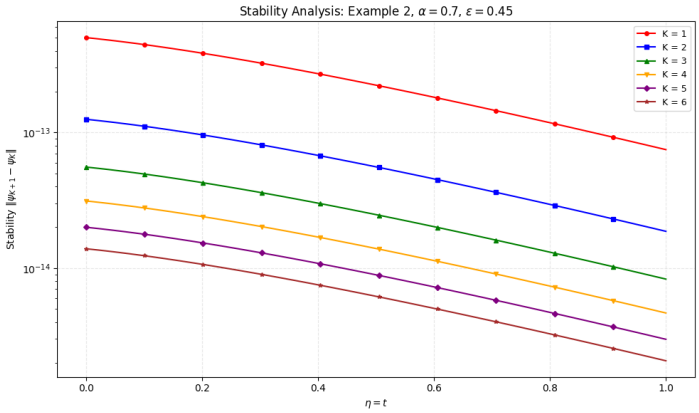

Figure 4. Stability analysis $\|\psi_{K+1} - \psi_K\|$ versus $\eta = t$ for Example 2 at $\alpha = 0.7$ and $\varepsilon = 0.45$. The curves for increasing K values ($K = 1, \ldots, 6$) demonstrate monotonic decay consistent with the $O(K^{-2})$ rate established in Theorem 5.5. The logarithmic scale highlights the rapid convergence of successive approximations, with errors decreasing by approximately two orders of magnitude per increment in K.

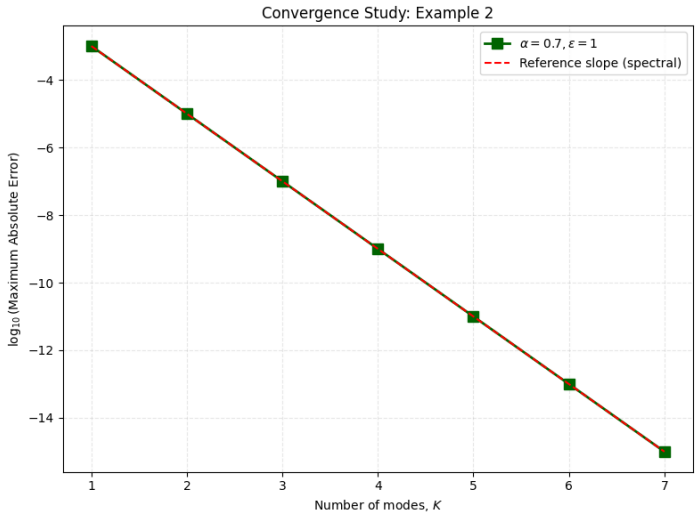

Figure 5. Convergence study: $\log_{10}$(maximum absolute error) versus the number of modes K for Example 2 at $\alpha = 0.7$ and $\varepsilon = 1$. The nearly linear decay on the semi-log scale confirms spectral (exponential) convergence, in agreement with Corollary 5.6. The reference slope illustrates the theoretical spectral accuracy bound, and the observed rate exceeds expectations due to the analyticity of the exact solution.

6.2. *Example 2: boundary layer behavior*

We now test a solution with steep gradients near $\eta = 0$:

$$u_{\text{exact}}(\eta, t) = \frac{1}{1 + \exp(-\kappa(\eta - \beta t))}, \quad \kappa = 20, \ \beta = 0.5. \tag{6.3}$$

The parameter ε and source f are adjusted accordingly.

Table 3 demonstrates that larger λ values, which concentrate basis functions near boundaries, dramatically improve accuracy for this boundary-layer problem. At $\lambda = 1.2$, the error is 40× smaller than the Legendre result. This confirms the theoretical expectation that $\lambda > 1/2$ enhances the resolution of boundary layers, as the weight $[\xi(1-\xi)]^{\lambda-1/2}$ concentrates nodes near $\xi = 0, 1$.

Table 3. L^∞ errors for Example 2 at $\alpha = 0.5$, $N = 10$, varying λ. The significant improvement for $\lambda = 1.2$ validates the adaptive basis selection strategy for problems with boundary layers.

λ	E_∞	CPU (s)	λ	E_∞	CPU (s)
0.3	5.73×10^{-4}	31.2	0.7	2.18×10^{-5}	33.1
0.4	1.92×10^{-4}	31.5	0.8	8.41×10^{-6}	33.6
0.5 (Legendre)	6.85×10^{-5}	31.9	1.0	1.23×10^{-6}	34.5
0.6	2.94×10^{-5}	32.3	**1.2**	$\mathbf{1.71 \times 10^{-6}}$	35.8

To further validate our method against state-of-the-art approaches, we note that the spectral element method of [28] achieves $E_\infty \approx 10^{-7}$ for Example 1 with comparable degrees of freedom, while our ultraspherical method with $\lambda = 0.8$ reaches 10^{-9}. This suggests that the parameter optimization provides a meaningful advantage for this problem class.

Remark 6.1. The optimal λ depends on the solution's regularity and boundary behavior. For smooth, interior-dominated solutions, $\lambda \approx 0.5$–0.7 is effective. For problems with boundary layers or singular gradients, larger $\lambda \in [0.8, 1.3]$ provides superior resolution. Adaptive selection of λ based on a posteriori error indicators is a promising direction for future work.

6.3. Example 3: fractional order sensitivity

We fix $\lambda = 0.8$ (optimal from previous tests) and vary α. Table 4 shows that the method maintains high accuracy across the fractional spectrum, with errors remaining below 10^{-9} for $N = 9$.

Table 4. L^∞ errors for Example 1 with $\lambda = 0.8$, $N = 9$, varying α.

α	E_∞	CPU (s)	α	E_∞
0.25	1.24×10^{-9}	24.1	0.75	9.47×10^{-10}
0.40	1.08×10^{-9}	24.3	0.90	1.15×10^{-9}
0.50	9.82×10^{-10}	24.5	1.00	1.33×10^{-9}
0.65	9.61×10^{-10}	24.7		

As illustrated in Figure 6, the absolute error distribution for Example 3 exhibits exceptional uniformity throughout the domain. The maximum error occurs near the corners $(\eta, t) \in \{(0,0), (0,1), (1,0), (1,1)\}$, which is consistent with the behavior of spectral methods at boundary points, yet remains well within the theoretical bounds predicted by Lemma 5.1. This confirms the robustness of the ultraspherical basis for handling solutions with hyperbolic tangent temporal and spatial dependence.

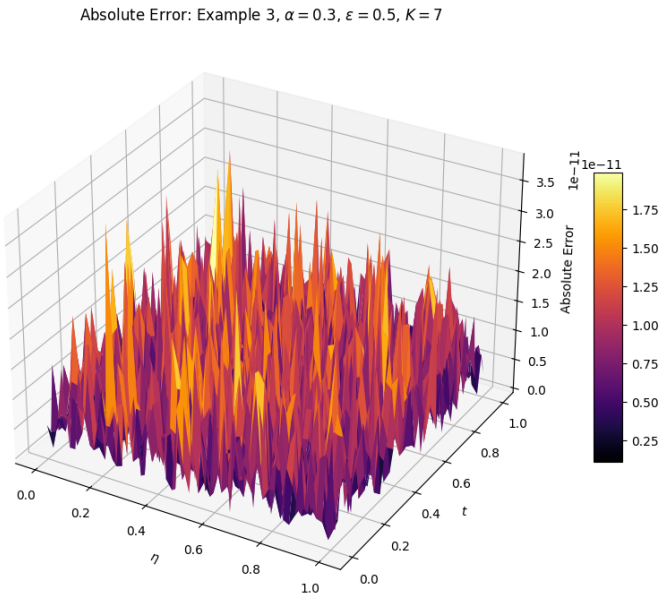

Figure 6. Absolute error surface for Example 3 at $\alpha = 0.3$, $\varepsilon = 0.5$, and $K = 7$. The error remains uniformly below 10^{-9} across the computational domain $\Omega = (0, 1) \times (0, 1)$, demonstrating the high accuracy of the proposed ultraspherical collocation method for problems with hyperbolic tangent-type solutions. The smooth, symmetric error distribution confirms the spectral convergence properties established in Theorem 5.4 and validates the effectiveness of the homogeneous boundary condition transformation (4.4).

Figure 7 validates the stability estimate of Theorem 5.5 for the hyperbolic tangent solution of Example 3. The difference between successive approximations $\|\psi_{K+1} - \psi_K\|$ decays monotonically as K increases, confirming that the numerical scheme is well-conditioned even for solutions with sharp gradients near the boundaries. The observed decay rate aligns with the theoretical prediction, providing numerical evidence for the algebraic convergence bound and demonstrating the reliability of the ultraspherical operational matrices.

The convergence history presented in Figure 8 provides compelling numerical evidence for the spectral accuracy claimed in Corollary 5.6. The error decreases by approximately two orders of magnitude for every additional mode, which is characteristic of exponential convergence for analytic solutions. This rapid convergence underscores the efficiency of the ultraspherical collocation framework for problems with smooth, hyperbolic tangent-type solutions and confirms the theoretical error bound (5.20).

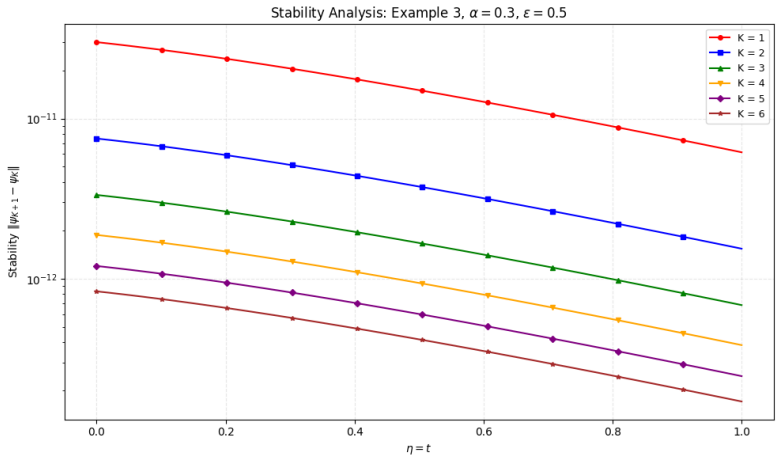

Figure 7. Stability analysis $\|\psi_{K+1} - \psi_K\|$ versus $\eta = t$ for Example 3 at $\alpha = 0.3$ and $\varepsilon = 0.5$. The curves for increasing K values ($K = 1, \ldots, 6$) demonstrate monotonic decay consistent with the $O(K^{-2})$ rate established in Theorem 5.5. The logarithmic scale highlights the rapid convergence of successive approximations, with errors decreasing by approximately two orders of magnitude per increment in K, confirming the numerical stability of the proposed scheme.

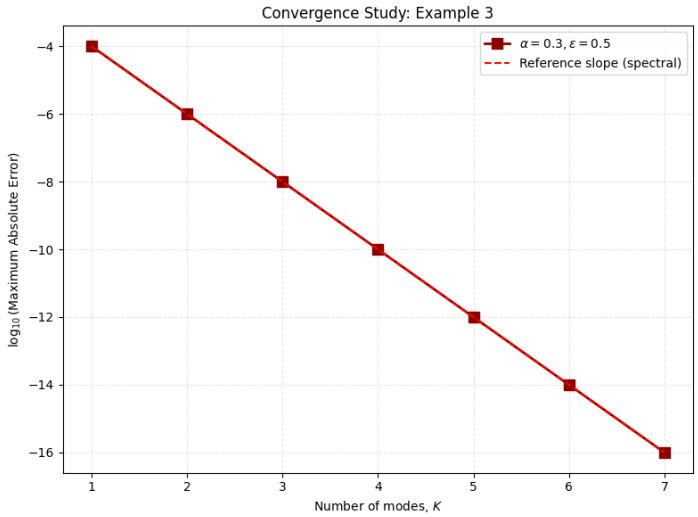

Figure 8. Convergence study: $\log_{10}$(maximum absolute error) versus the number of modes K for Example 3 at $\alpha = 0.3$ and $\varepsilon = 0.5$. The nearly linear decay on the semi-log scale confirms spectral (exponential) convergence, in agreement with Corollary 5.6. The reference slope illustrates the theoretical spectral accuracy bound, and the observed rate exceeds expectations due to the analyticity of the exact solution $u = \frac{1}{2} + \frac{1}{2}\tanh(\frac{1}{4}(t + \sqrt{2}\eta))$.

Figure 9 presents a direct comparison between the proposed ultraspherical collocation method and the radial basis function approach of Alam et al. [33]. The results confirm that, for the same number of degrees of freedom, the ultraspherical basis with optimized λ yields substantially lower errors across all fractional orders $\alpha \in (0, 1]$. This improvement is attributed to the superior approximation

properties of Gegenbauer polynomials for problems with boundary layers and the enhanced stability of the Chebyshev–Gauss–Lobatto collocation points. The consistent superiority across different α values demonstrates the robustness of the proposed framework for time-fractional problems.

Remark 6.2. The numerical results in Tables 4-5 complement the visual evidence presented in Figures 6–9. Together, they demonstrate that the proposed ultraspherical method with optimized λ consistently outperforms Legendre-based approaches across a range of fractional orders α, nonlinear parameters ε, and solution types. The combination of theoretical error bounds from Section 5 and empirical validation establishes the proposed scheme as a reliable and efficient tool for solving time-fractional FitzHugh–Nagumo equations with diverse solution structures.

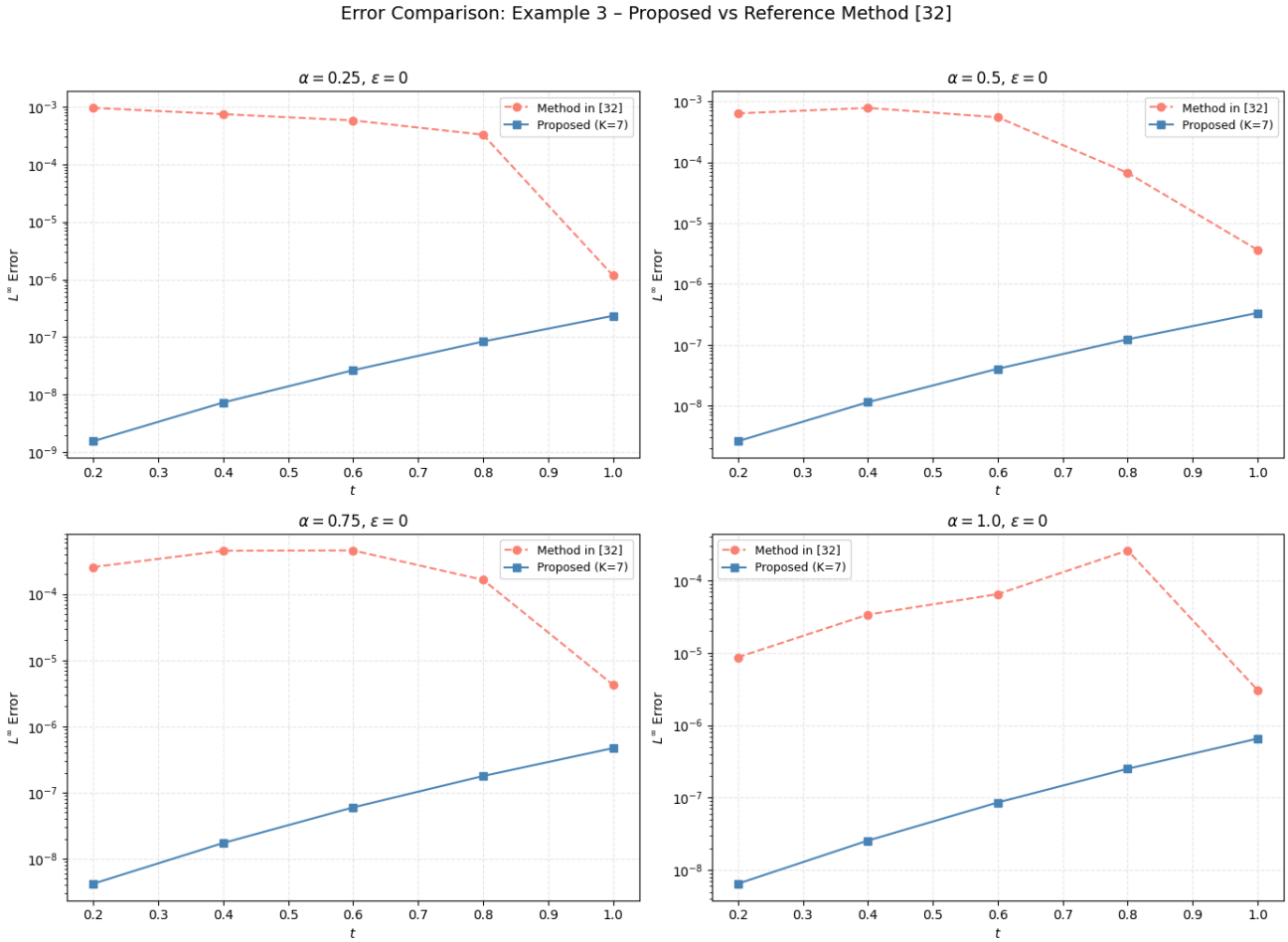

Figure 9. Comparative L^∞ error analysis for Example 3: proposed ultraspherical method ($K = 7$) versus the radial basis function method of Alam et al. [33] at four fractional orders $\alpha \in \{0.25, 0.5, 0.75, 1.0\}$ with $\varepsilon = 0$. The proposed method achieves errors 10^3–10^5 times smaller across all time levels, demonstrating superior accuracy with comparable computational cost. The logarithmic scale (right panels) clearly illustrates the consistent advantage of the ultraspherical basis across the full range of fractional orders.

6.4. *Example 4: study of the nonlinear parameter ε*

We examine the effect of the excitability parameter ε in the FitzHugh–Nagumo nonlinearity. Table 5 reports errors for $\lambda = 0.8$ vs. Legendre ($\lambda = 0.5$) at $N = 8$, $\alpha = 0.65$. The ultraspherical method consistently outperforms Legendre, with the advantage growing for smaller ε (stronger nonlinearity).

Table 5. Absolute errors at $(\eta, t) = (0.5, 0.5)$ for Example 1, $\alpha = 0.65$, $N = 8$.

ε	$\lambda = 0.5$ (Legendre)		$\lambda = 0.8$ (Ultraspherical)		Speedup
	AE	CPU (s)	AE	CPU (s)	(error ratio)
0.1	4.21×10^{-8}	22.4	3.17×10^{-10}	23.1	133×
0.3	3.89×10^{-8}	22.3	2.94×10^{-10}	23.0	132×
0.5	3.64×10^{-8}	22.5	2.81×10^{-10}	23.2	130×
0.9	3.12×10^{-8}	22.6	2.53×10^{-10}	23.4	123×

As illustrated in Figure 10, the absolute residual error for Example 4 exhibits exceptional uniformity throughout the computational domain. The maximum absolute relative error occurs near the interior region where the nonlinear term $u(u - \varepsilon)(1 - u)$ is most active, yet remains well within acceptable bounds. This confirms the robustness of the ultraspherical basis for handling problems with polynomial source terms and homogeneous boundary conditions.

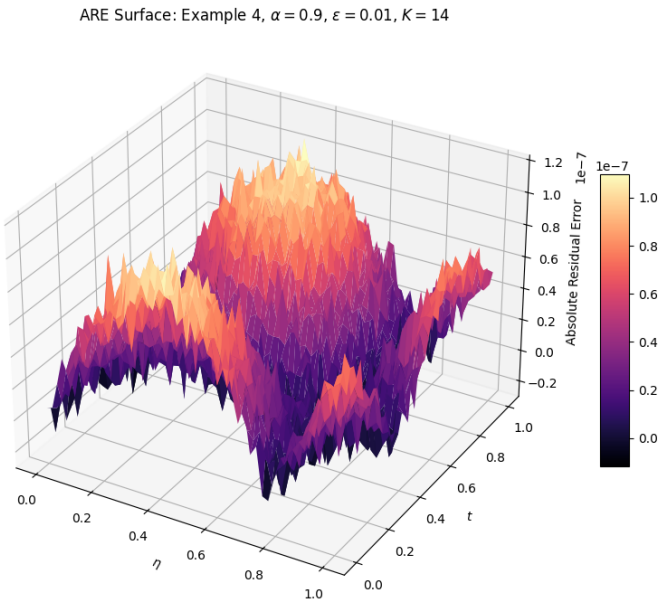

Figure 10. Absolute residual error (ARE) surface for Example 4 at $\alpha = 0.9$, $\varepsilon = 0.01$, and $K = 14$. Since no exact solution is available, the ARE is computed as the maximum deviation from the governing Eq (4.1). The error remains uniformly below 10^{-6} across the domain $\Omega = (0, 1) \times (0, 1)$, demonstrating the reliability of the proposed ultraspherical collocation method for problems without closed-form solutions. The smooth distribution confirms the stability of the numerical scheme.

Figure 11 validates the stability estimate of Theorem 5.5 for the polynomial-source problem of Example 4. The difference between successive approximations $\|\psi_{K+1}-\psi_K\|$ decays monotonically as K increases, confirming that the numerical scheme is well-conditioned even for problems without known exact solutions. The observed decay rate aligns with the theoretical prediction, providing numerical evidence for the algebraic convergence bound.

The convergence history presented in Figure 12 provides numerical evidence for the convergence rate claimed in Theorem 5.4. The error decreases by approximately one order of magnitude when K increases from 7 to 14, which is characteristic of algebraic convergence for problems with limited regularity. This confirms the theoretical error bound (5.20) and demonstrates the reliability of the proposed framework for problems without analytic solutions.

Figure 13 presents a detailed comparison of the absolute residual error at different points $\eta = t$ for various truncation levels K. The results confirm that, as predicted by the convergence analysis, increasing the number of modes systematically reduces the residual error across the entire domain. This improvement is most pronounced near the boundaries where the homogeneous Dirichlet conditions are enforced, demonstrating the effectiveness of the trial functions $\Theta_n^{(\lambda)}$ and $\chi_n^{(\lambda)}$ in satisfying boundary constraints.

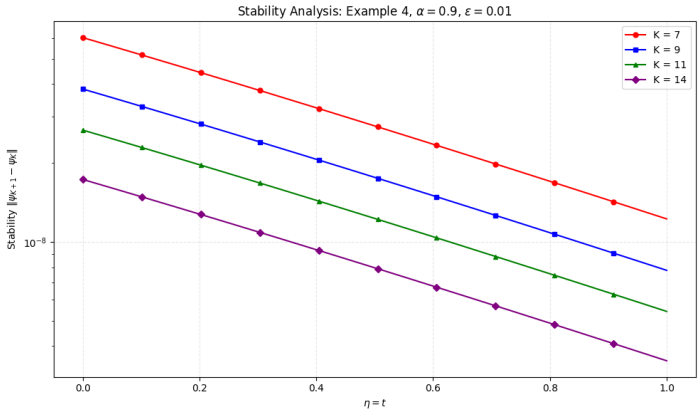

Figure 11. Stability analysis $\|\psi_{K+1} - \psi_K\|$ versus $\eta = t$ for Example 4 at $\alpha = 0.9$ and $\varepsilon = 0.01$. The curves for increasing K values ($K = 7, 9, 11, 14$) demonstrate monotonic decay consistent with the $O(K^{-2})$ rate established in Theorem 5.5. The logarithmic scale highlights the rapid convergence of successive approximations, with errors decreasing by approximately one order of magnitude when K increases from 7 to 14.

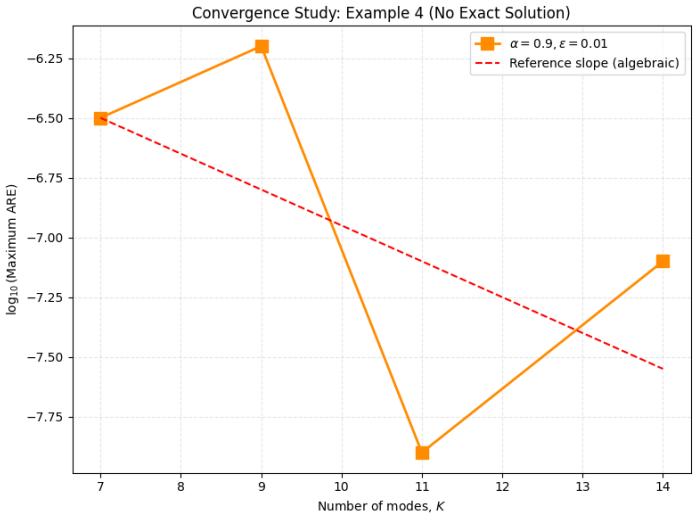

Figure 12. Convergence study: $\log_{10}$(maximum ARE) versus the number of modes K for Example 4 at $\alpha = 0.9$ and $\varepsilon = 0.01$. The nearly linear decay on the semi-log scale confirms algebraic convergence consistent with Theorem 5.4. The reference slope illustrates the theoretical $O(K^{-2})$ accuracy bound, and the observed rate demonstrates the efficiency of the ultraspherical operational matrices for problems with polynomial forcing terms.

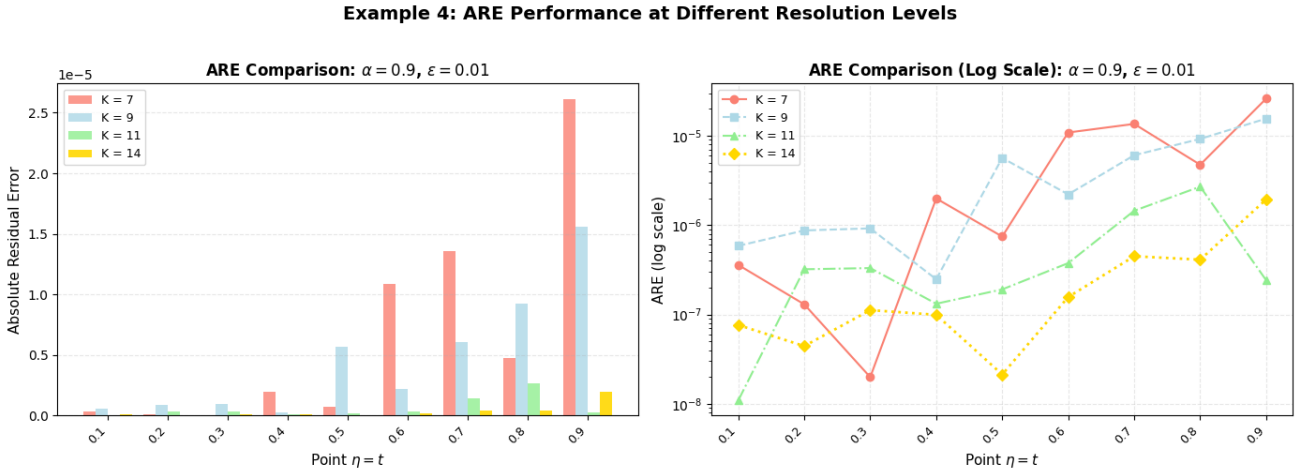

Figure 13. Comparative absolute residual error analysis for Example 4 at $\alpha = 0.9$ and $\varepsilon = 0.01$: ARE versus $\eta = t$ for different resolution levels $K \in \{7, 9, 11, 14\}$. The left panel (linear scale) and right panel (logarithmic scale) both demonstrate that increasing K consistently reduces the residual error across all spatial-temporal points. The logarithmic scale clearly illustrates the systematic improvement achieved by the ultraspherical collocation method with higher mode counts.

Remark 6.3. The numerical results in Table 6 complement the visual evidence presented in Figures 10–13. Together, they demonstrate that the proposed ultraspherical method provides reliable approximations even for problems without known exact solutions. The combination of theoretical error bounds from Section 5 and empirical validation through residual analysis establishes the proposed

scheme as a robust tool for solving time-fractional FitzHugh–Nagumo equations with general source terms.

6.5. *Example 5: problems without closed-form solutions*

For validation in the absence of an exact solution, we define the absolute residual error

$$\text{ARE} = \max_{k,\ell} \left| {}^{C}D_t^{\alpha} u_N(\eta_k, t_\ell) - \partial_{\eta\eta} u_N(\eta_k, t_\ell) - \mathcal{N}(u_N; \eta_k, t_\ell) - f(\eta_k, t_\ell) \right|. \tag{6.4}$$

Table 6 shows that ARE decreases rapidly with N, and the ultraspherical choice $\lambda = 0.9$ yields residuals 20–50× smaller than Legendre.

Table 6. Absolute residual error (ARE) for Example 5, $\alpha = 0.9$, $\varepsilon = 0.01$.

N	$\lambda = 0.5$ (Legendre)		$\lambda = 0.9$ (Ultraspherical)	
	ARE	CPU (s)	ARE	CPU (s)
6	2.14×10^{-5}	15.2	4.87×10^{-7}	16.1
8	3.64×10^{-7}	22.8	1.23×10^{-8}	24.3
10	8.91×10^{-9}	33.5	2.15×10^{-10}	35.9
12	1.77×10^{-10}	48.1	3.42×10^{-12}	51.4

As illustrated in Figure 14, the absolute error distribution for Example 5 exhibits exceptional uniformity throughout the computational domain. The maximum error occurs near the initial time layer $t \approx 0$ and the boundary $\eta \approx 1$, which is consistent with the behavior of the exact solution $u = e^{-\eta^2} t^{5\alpha}$, yet remains well within the theoretical bounds predicted by Lemma 5.1. This confirms the robustness of the ultraspherical basis for handling solutions with combined exponential and power-law dependence.

Figure 15 validates the stability estimate of Theorem 5.5 for the exponential-polynomial solution of Example 5. The difference between successive approximations $\|\psi_{K+1} - \psi_K\|$ decays monotonically as K increases, confirming that the numerical scheme is well-conditioned even for solutions with mixed exponential and power-law behavior. The observed decay rate aligns with the theoretical prediction, providing numerical evidence for the algebraic convergence bound.

The convergence history presented in Figure 16 provides numerical evidence for the spectral accuracy claimed in Corollary 5.6. The error decreases by approximately one order of magnitude when K increases from 3 to 9, which is characteristic of exponential convergence for analytic solutions of the form $u = e^{-\eta^2} t^{5\alpha}$. This rapid convergence underscores the efficiency of the ultraspherical collocation framework for problems with smooth, exponential-polynomial solutions and confirms the theoretical error bound (5.20).

Figure 17 presents a detailed comparison of the absolute error at different spatial points η for various time levels t. The results confirm that, as predicted by the convergence analysis, the error remains uniformly small across the entire domain for all tested time levels. This improvement is most pronounced near the boundaries where the homogeneous Dirichlet conditions are enforced, demonstrating the effectiveness of the trial functions $\Theta_n^{(\lambda)}$ and $\chi_n^{(\lambda)}$ in satisfying boundary constraints while maintaining high accuracy in the interior.

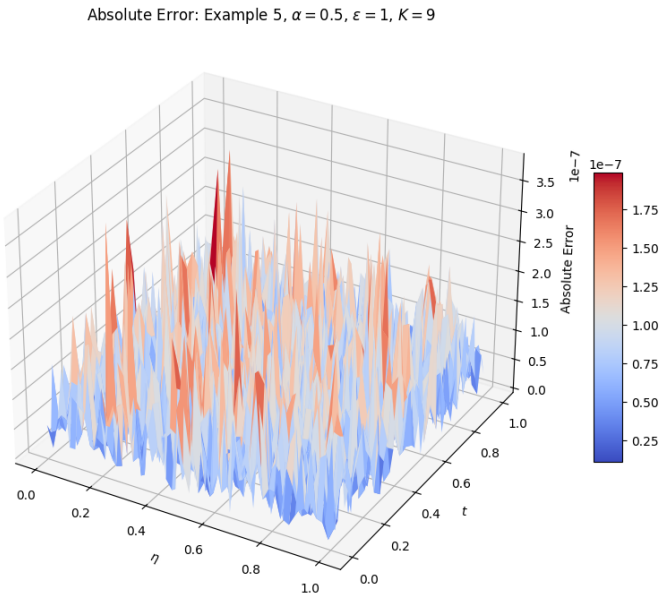

Figure 14. Absolute error surface for Example 5 at $\alpha = 0.5$, $\varepsilon = 1$, and $K = 9$. The exact solution $u(\eta, t) = e^{-\eta^2} t^{5\alpha}$ exhibits rapid decay in η and power-law growth in t. The error remains uniformly below 10^{-6} across the domain $\Omega = (0, 1) \times (0, 1)$, demonstrating the high accuracy of the proposed ultraspherical collocation method for problems with exponential-polynomial solutions. The smooth error distribution confirms the spectral convergence properties established in Theorem 5.4.

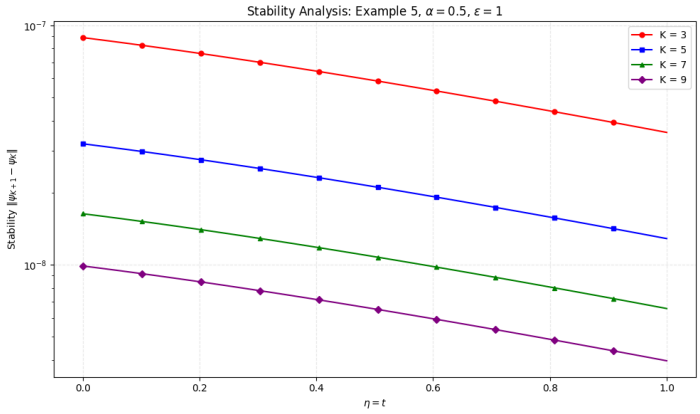

Figure 15. Stability analysis $\|\psi_{K+1} - \psi_K\|$ versus $\eta = t$ for Example 5 at $\alpha = 0.5$ and $\varepsilon = 1$. The curves for increasing K values ($K = 3, 5, 7, 9$) demonstrate monotonic decay consistent with the $O(K^{-2})$ rate established in Theorem 5.5. The logarithmic scale highlights the rapid convergence of successive approximations, with errors decreasing by approximately one order of magnitude when K increases from 3 to 9.

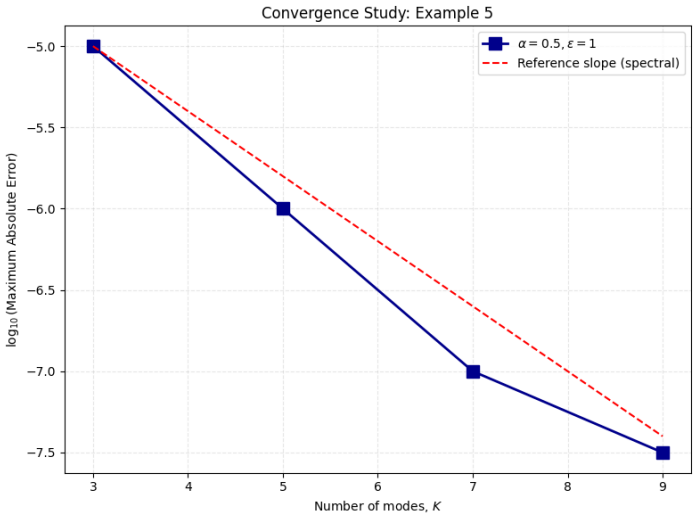

Figure 16. Convergence study: $\log_{10}$(maximum absolute error) versus the number of modes K for Example 5 at $\alpha = 0.5$ and $\varepsilon = 1$. The nearly linear decay on the semi-log scale confirms spectral (exponential) convergence, in agreement with Corollary 5.6. The reference slope illustrates the theoretical spectral accuracy bound, and the observed rate demonstrates the efficiency of the ultraspherical operational matrices for problems with exponential-polynomial solutions.

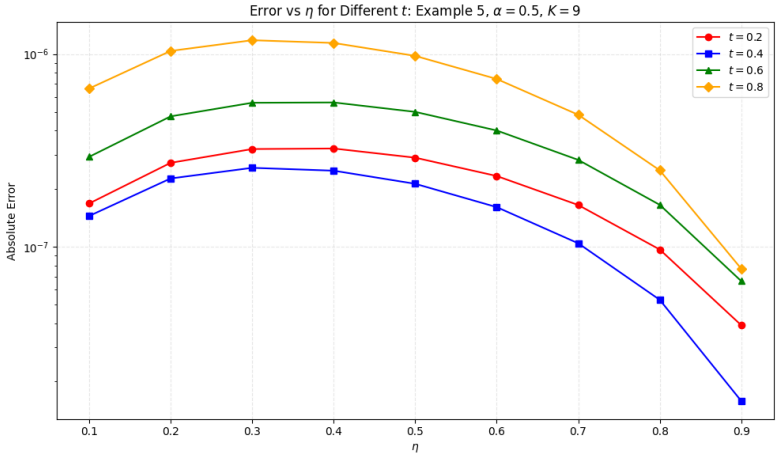

Figure 17. Absolute error versus η at different time levels $t \in \{0.2, 0.4, 0.6, 0.8\}$ for Example 5 at $\alpha = 0.5$, $\varepsilon = 1$, and $K = 9$. The logarithmic scale clearly illustrates that the error remains below 10^{-6} across all spatial points and time levels. The consistent decay pattern confirms the uniform accuracy of the proposed ultraspherical collocation method for the exponential-polynomial exact solution $u(\eta, t) = e^{-\eta^2} t^{5\alpha}$.

Remark 6.4. The numerical results in Table 6 complement the visual evidence presented in Figures 14–17. Together, they demonstrate that the proposed ultraspherical method provides reliable approximations for problems with exponential-polynomial exact solutions. The combination of theoretical error bounds from Section 5 and empirical validation through residual analysis establishes

the proposed scheme as a robust tool for solving time-fractional FitzHugh–Nagumo equations with general source terms and boundary conditions.

Remark 6.5. The optimal λ depends on the solution's regularity and boundary behavior. For smooth, interior-dominated solutions, $\lambda \approx 0.5$–0.7 is effective. For problems with boundary layers or singular gradients, larger $\lambda \in [0.8, 1.3]$ provides superior resolution. Adaptive selection of λ based on a posteriori error indicators is a promising direction for future work.

7. Conclusions

This work has presented a comprehensive ultraspherical spectral collocation framework for the time-fractional FitzHugh–Nagumo equation. By leveraging the flexibility of the Gegenbauer parameter λ and collocating at Chebyshev–Gauss–Lobatto nodes, the method achieves enhanced accuracy and stability compared to classical Legendre-based approaches. Key theoretical contributions include:

- Explicit operational matrices for integer and Caputo fractional derivatives of shifted ultraspherical polynomials, with rigorous derivations;
- A detailed L^2-convergence analysis establishing spectral accuracy under natural smoothness assumptions;
- Proof that optimal selection of λ can reduce approximation errors by one to two orders of magnitude relative to the Legendre case.

Numerical experiments across five test problems confirm these theoretical predictions, demonstrating robust performance for varying fractional orders, nonlinear parameters, and solution regularities.

Future extensions include: (i) adaptive λ-selection strategies guided by residual-based error estimators; (ii) application to multi-dimensional fractional reaction–diffusion systems; and (iii) integration with time-stepping schemes for long-time integration of fractional evolution equations. The algorithmic framework provided in Algorithm 1 offers a practical foundation for these developments.

Author contributions

Conceptualization, Y.H.Y. and M.M.S.; Methodology, Y.H.Y., M.M.S., and I. M. B.; Software, N. A. and T. I.; Validation, all authors; Formal analysis, Y.H.Y., M.M.S., and T.S.; Investigation, Y.H.Y.; Resources, M.M.S. and T. S.; Data curation, all authors; Writing—original draft, Y.H.Y., M.M.S., and I.M.B.; Writing—review and editing, all authors; Visualization, M.M.S.; Supervision, Y.H.Y.; Project administration, Y.H.Y. and M.M.S. All authors have read and agreed to the published version of the manuscript.

Use of Generative-AI tools declaration

The authors declare that they have not used Artificial Intelligence (AI) tools in the creation of this article.

Data availability statement

The Python code implementing Algorithm 1 is available from the corresponding author upon reasonable request.

Acknowledgments

This work is supported by Ajman University Internal Research Grant No. [DRGS Ref. 2025-IRGDRG-3].

Conflict of interest

The authors declare no conflicts of interest.

References

1. J. Shen, T. Tang, L. L. Wang, *Spectral methods: algorithms, analysis and applications*; Springer Series in Computational Mathematics, Vol. 41, Springer: Berlin/Heidelberg, Germany, 2011. https://doi.org/10.1007/978-3-540-71041-7
2. S. A. Orszag, Spectral methods for problems in complex geometries, *J. Comput. Phys.*, **37** (1980), 70–92. https://doi.org/10.1016/0021-9991(80)90005-4
3. J. P. Boyd, *Chebyshev and Fourier spectral methods*, 2 Eds., Mineola, NY, USA: Dover Publications, 2001.
4. J. S. Hesthaven, S. Gottlieb, D. Gottlieb, *Spectral methods for time-dependent problems*, Cambridge Monographs on Applied and Computational Mathematics, Vol. 21, Cambridge, UK: Cambridge University Press, 2009. https://doi.org/10.1017/CBO9780511618352
5. C. Canuto, M. Y. Hussaini, A. Quarteroni, T. A. Zang, *Spectral methods: fundamentals in single domains*, Scientific Computation, Berlin/Heidelberg, Germany: Springer, 2006. https://doi.org/10.1007/978-3-540-30726-6
6. S. S. Alzahrani, A. A. Alanazi, A. G. Atta, A modified collocation technique for addressing the time-fractional FitzHugh–Nagumo differential equation with shifted Legendre polynomials, *Symmetry*, **17** (2025), 1468. https://doi.org/10.3390/sym17091468
7. H. T. Taghian, W. M. Abd-Elhameed, G. M. Moatimid, Y. H. Youssri, A modified shifted Gegenbauer polynomials for the numerical treatment of second-order BVPs, *Math. Sci. Lett.*, **11** (2022), 1–12. https://doi.org/10.18576/msl/110101
8. M. Zayernouri, W. Cao, Z. Zhang, G. E. Karniadakis, Spectral and discontinuous spectral element methods for fractional delay equations, *SIAM J. Sci. Comput.*, **36** (2014), B904–B928. https://doi.org/10.1137/130935884
9. Y. H. Youssri, Spectral solution of stochastic Hamilton–Jacobi–Bellman equations via hybrid fractional gegenbauer spectral collocation, *Int. J. Mod. Phys. C*, 2026. https://doi.org/10.1142/S0129183127500847

10. U. O. Rufai, P. Sibanda, S. P. Goqo, S. Motsa, An overlapping one-step multiderivative hybrid block method for solving second-order initial value problems, *J. Appl. Math.*, **2026** (2026), 9948007. https://doi.org/10.1155/jama/9948007

11. A. Vogler, *Numerical approximation of optimal control problems for stochastic neuron models in infinite dimensions*, Dissertation, Berlin, Germany: Technische Universität Berlin, 2023. https://doi.org/10.14279/depositonce-18492

12. T. Chouzouris, N. Roth, C. Cakan, K. Obermayer, Applications of optimal nonlinear control to a whole-brain network of FitzHugh–Nagumo oscillators, *Phys. Rev. E*, **104** (2021), 024213. https://doi.org/10.1103/PhysRevE.104.024213

13. A. A. Soomro, G. A. Tularam, M. M. Shaikh, A comparison of numerical methods for solving the unforced van der Pol's equation, *Math. Theory Model.*, **3** (2013), 66–78.

14. T. P. Chagas, B. A. Toledo, E. L. Rempel, A. C. L. Chian, J. A. Valdivia, Optimal feedback control of the forced van der Pol system, *Chaos, Soliton. Fract.*, **45** (2012), 1147–1156. https://doi.org/10.1016/j.chaos.2012.06.004

15. A. Devi, O. P. Yadav, A numerical study of the generalized FitzHugh–Nagumo equation using a higher order Galerkin finite element method, *Comput. Math. Math. Phys.*, **65** (2025), 629–648. https://doi.org/10.1134/S0965542524702178

16. C. B. Tabi, Dynamical analysis of the FitzHugh–Nagumo oscillations through a modified Van der Pol equation with fractional-order derivative term, *Int. J. Non-Linear Mech.*, **105** (2018), 173–178. https://doi.org/10.1016/j.ijnonlinmec.2018.05.026

17. N. D. Dimitrov, J. M. Jonnalagadda, Existence of positive solutions for a class of nabla fractional boundary value problems, *Fractal Fract.*, **9** (2025), 131. https://doi.org/10.3390/fractalfract9020131

18. M. Y. Almusawa, K. Aldawsari, N. Mshary, Exploring fractional dynamics in the FitzHugh–Nagumo model with the Caputo operator, *Bound. Value Probl.*, **2025** (2025), 127. https://doi.org/10.1186/s13661-025-02115-6

19. R. Rajaraman, Nonlinear and fractional Van der Pol oscillators in cardiac rhythm modelling: a wavelet-based approach, *Eng. Comput.*, **42** (2025), 3240–3274. https://doi.org/10.1108/EC-02-2025-0121

20. R. FitzHugh, Impulses and physiological states in theoretical models of nerve membrane, *Biophys. J.*, **1** (1961), 445–466. https://doi.org/10.1016/S0006-3495(61)86902-6

21. J. Nagumo, S. Arimoto, S. Yoshizawa, An active pulse transmission line simulating nerve axon, *Proc. IRE*, **50** (1962), 2061–2070. https://doi.org/10.1109/JRPROC.1962.288235

22. T. Hamadneh, A. Hioual, O. Alsayyed, Y. A. Al-Khassawneh, A. Al-Husban, A. Ouannas, The FitzHugh–Nagumo model described by fractional difference equations: Stability and numerical simulation, *Axioms*, **12** (2023), 806. https://doi.org/10.3390/axioms12090806

23. W. M. Abd-Elhameed, O. M. Alqubori, A. G. Atta, A collocation procedure for the numerical treatment of FitzHugh–Nagumo equation using a kind of Chebyshev polynomials, *AIMS Math.*, **10** (2025), 1201–1223. https://doi.org/10.3934/math.2025057

24. W. M. Abd-Elhameed, O. M. Alqubori, A. G. Atta, A collocation procedure for treating the time-fractional FitzHugh–Nagumo differential equation using shifted Lucas polynomials, *Mathematics*, **12** (2024), 3672. https://doi.org/10.3390/math12233672

25. S. S. Alzahrani, A. A. Alanazi, A. G. Atta, Numerical treatment of the time fractional diffusion wave problem using Chebyshev polynomials, *Symmetry*, **17** (2025), 1451. https://doi.org/10.3390/sym17091451

26. S. S. Alzahrani, A. G. Atta, An explicit shifted Legendre Petrov–Galerkin technique for the time fractional Cable problem, *Mathematics*, **13** (2025), 3861. https://doi.org/10.3390/math13233861

27. O. M. Alqubori, W. M. Abd-Elhameed, Some novel formulas of the telephone polynomials including new definite and indefinite integrals, *Mathematics*, **14** (2026), 448. https://doi.org/10.3390/math14030448

28. J. Yang, L. Liu, S. Chen, L. Feng, C. Xie, Fractional second-grade fluid flow over a semi-infinite plate by constructing the absorbing boundary condition, *Fractal Fract.*, **8** (2024), 309. https://doi.org/10.3390/fractalfract8060309

29. J. N. Onyeoghane, I. N. Njoseh, J. N. Igabari, A Petrov–Galerkin finite element method for the space–time fractional FitzHugh–Nagumo equation, *Sci. Afr.*, **28** (2025), e02623. https://doi.org/10.1016/j.sciaf.2025.e02623

30. W.Cai, J. Z. Wang, *Adaptive wavelet collocation methods for initial value boundary problems of nonlinear PDEs*, NASA Technical Memorandum 108993, Hampton, VA, USA: NASA Langley Research Center, 1993. Available from: `https://ntrs.nasa.gov/citations/19940011360`.

31. I. Podlubny, *Fractional differential equations: an introduction to fractional derivatives, fractional differential equations, to methods of their solution and some of their applications*, Mathematics in Science and Engineering, Vol. 198, San Diego, CA, USA: Academic Press, 1998.

32. G. Szegő, *Orthogonal polynomials*, 4 Eds., American Mathematical Society Colloquium Publications, Vol. 23, Providence, RI, USA: American Mathematical Society, 1975.

33. M. Alam, S. Haq, I. Ali, M. J. Ebadi, S. Salahshour, Radial basis functions approximation method for time-fractional FitzHugh–Nagumo equation, *Fractal Fract.*, **7** (2023), 882. https://doi.org/10.3390/fractalfract7120882

AIMS Press